Landsvirkjun

Geodetic Observations and Surface Deformation at Krafla mid 2018-2020

Status Report December 2020

Landsvirkjun

Geodetic Observations
and Surface Deformation at Krafla
mid 2018–2020

Status Report December 2020

![Landsvirkjun]

Key Page

LV report no:	LV-2020-036		**Date:**	December 2020

Number of pages:	46	**Copies:** 1	**Distribution:**	☒ **On www.lv.is** ☒ **Open** ☐ **Limited until**

Abstract: Following continuous subsidence in the Krafla caldera for several years, inferred inflation of the caldera based on InSAR data began in the middle of 2018. The Institute of Earth Sciences (IES), University of Iceland, Iceland GeoSurvey (ÍSOR) and Landsvirkjun carried out various geoscientific studies to improve the understanding of the ongoing ground deformation. Gravity and GNSS measurements were performed at permanent sites in late 2019 and a GNSS survey in the Krafla, Bjarnarflag and Þeistareykir areas in summer 2020. Seismic release during this time was studied as well.

The changes in ground deformation pattern are either related to magmatic or geothermal processes or a combination of both. The inferred depth of the pressure source from point source modelling, based on simplified assumptions, is found to be at 2.5 km depth or between 2.3 and 3.1 km with 95% confidence limits. However, considering modelling simplifications and uncertainties, the source of pressure change might originate in the magmatic or the geothermal system, or directly at the brittle-ductile boundary where the geothermal and magmatic systems meet. If the pressure change is of geothermal origin, it can either be due to natural geothermal processes or changes in the geothermal utilization. In recent years both the amount of fluid extraction and the amount and location of fluid re-injection into wells have changed, with potential influence on deformation patterns.

Approved by Landsvirkjun's project manager

Project manager's signature	Reviewed by
Gylfi Páll Hersir (signature)	Ólafur G. Flóvenz
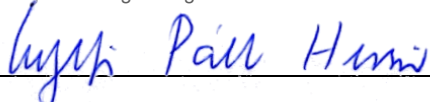
Table of contents

List of tables

List of figures

1 Introduction

This report documents work aimed at understanding ongoing ground deformation in the Krafla caldera, in relation to inferred inflation of the caldera beginning in 2018. It is a continuation of studies of ground deformation at geothermal areas in North-East Iceland, carried out in collaboration between Institute of Earth Sciences (IES), University of Iceland, Iceland GeoSurvey (ÍSOR) and Landsvirkjun. The work described here also follows a meeting between representatives from Landsvirkjun, IES and ÍSOR on November the 6th, 2019, when it was proposed to measure gravity and GNSS at permanent sites where measurements had been done before, i.e. along the main road towards north in the direction of the power plant and to Víti, and from there to the west across Leirhnjúkur where the center of the uplift is found according to recent InSAR measurements (Drouin et al., 2019). The proposed measurements are discussed in a Memo from ÍSOR to Landsvirkjun dated November the 7th (Hersir et al., 2019b). The survey and its results have already been discussed in a short report in Icelandic (Hersir et al., 2019a). Furthermore, it was proposed to see if there had been some changes in the pattern of seismic release during this time.

In the following chapters, the name of scientists contributing to the respective chapters are indicated with their initials in brackets.

2 Surface deformation – InSAR (VD)

Synthetic Aperture Radar Interferometry (InSAR) of Sentinel-1 images was used to infer the deformation at Krafla between summer 2015 and summer 2020. Only summer images (i.e. from mid-June to end of September) are used because measurements are not possible when the ground is covered with snow. Line-of-sight (LOS) displacements were calculated for the three Sentinel-1 tracks covering the area: T9, T111, and T147. The velocity fields derived from the displacements show a clear deviation of the 2018-2020 deformation rate from the "usual" 2015-2018 deformation rate within the Krafla caldera (Figure 1). We decomposed the LOS velocities of the three tracks to extract the approximate vertical (near-Up) velocities for having a better visualization and understanding of the deformation. The velocities between summers for the pre-inflation period (2015-2018) and the inflation periods (2018-2019 and 2019-2020) are shown in Figure 2.

The area of maximum vertical deformation appears to be in-between Leirhnjúkur and the IDDP-1 well. This area was subsiding at a fairly constant rate between summer 2015 and summer 2018, then started to uplift between summer 2018 and summer 2019 and continued to uplift at a slightly lower rate between summer 2019 and summer 2020 (Figure 3).
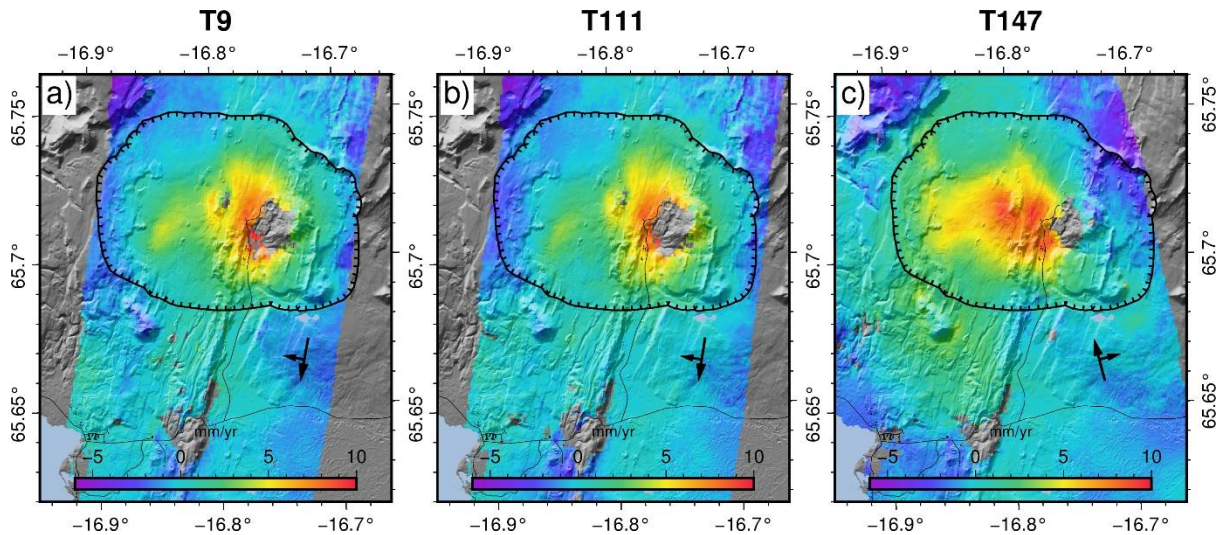
Figure 1. *InSAR LOS velocities [mm/yr] showing the deviation of the 2018-2020 velocities from the 2015-2018 velocities for three Sentinel-1 tracks: two descending (T9 and T111) and one ascending (T147). The heading and look direction of the satellite tracks is shown by the black arrows. Background shows shaded topography, the Krafla caldera boundary (comb line), and roads (black lines).*
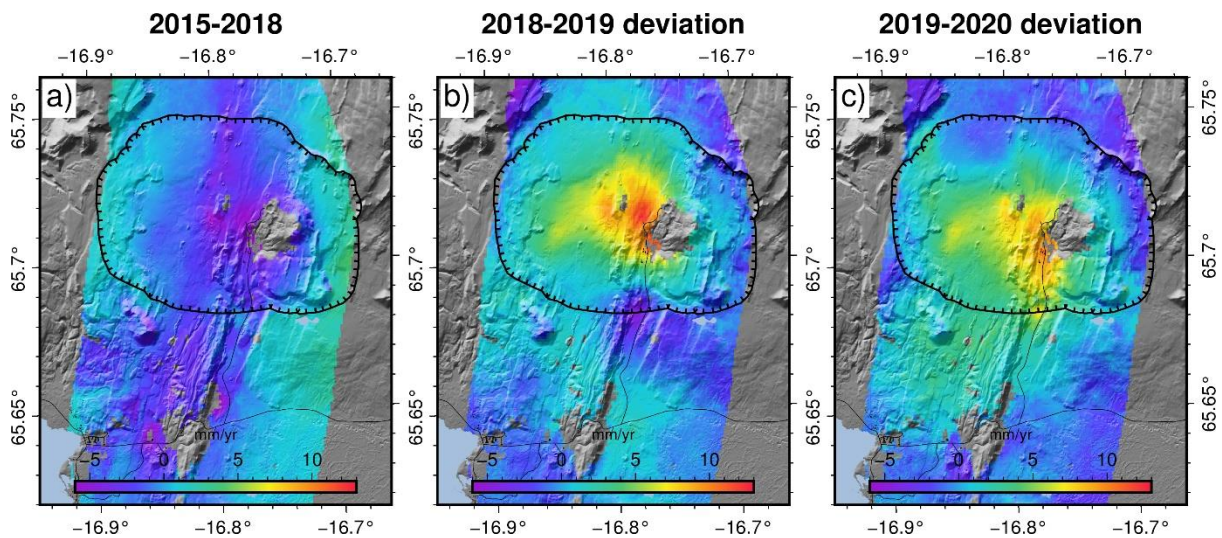
Figure 2. *Near-Up velocities [mm/yr] derived from the decomposition of the LOS velocities from the three Sentinel-1 tracks (T9, T111, T147). a) The "usual" annual rate of deformation in Krafla inferred from 2015-2018 images. b) The deviation of the deformation rate between summer 2018 and summer 2019 from the "usual" 2015-2018 rate. c) The deviation of the deformation rate between summer 2019 and summer 2020 from the "usual" 2015-2018 rate. Background is the same as in Figure 1.*
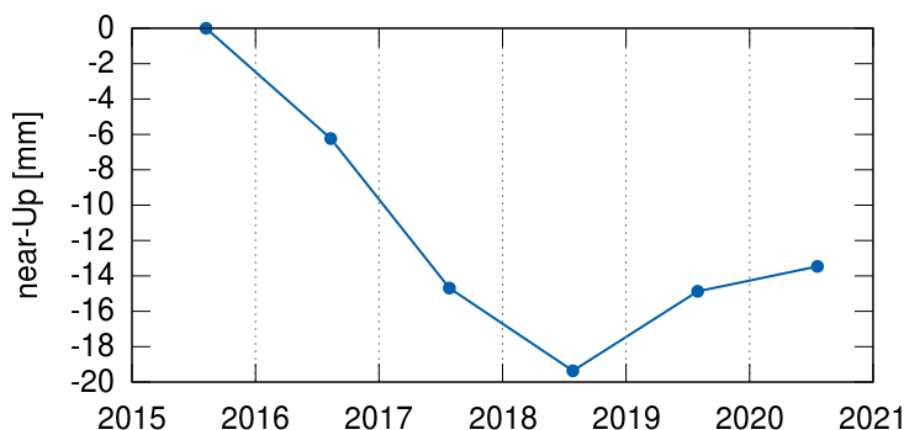
Figure 3. *Time-series of height changes in the area between Leirhnjúkur and IDDP-1 well relative to 2015.*

The main observations that can be derived from the results are the following:

2015-2018 (Fig. 2a)

- 5-8 mm/yr subsidence in Krafla and Bjarnarflag: likely caused by geothermal utilization (Drouin et al., 2017).
- 5 mm/yr subsidence along the fissure swarm: likely caused by rifting along a weak zone in the plate boundary under the influence of plate spreading.

2018-2019 deviation (Fig. 2b)

- 10-13 mm/yr uplift between Leirhnjúkur and IDDP-1: potential magma movements.
- 5-6 mm/yr subsidence south of Hvíthólar: possibly caused by variation in steam/water extraction.

2019-2020 deviation (Fig. 2c)

- 8-11 mm/yr uplift near Leirhnjúkur and the Krafla power station: less uplift than in 2018-2019 but a bit more to the south, near the power station.
- End of the subsidence south of Hvíthólar.

It is considered that background deformation happening for 2015-2018 (Fig. 2a) did also occur for 2018-2019 and 2019-2020. Therefore, the difference velocity fields shown in Fig. 2b and 2c are inferred to be a result of processes taking place in addition to those that create the background deformation.

3 Gravity and GNSS-measurements (IÞM, GPH, KÁ)

Gravity was measured in Krafla by ÍSOR on November 11th to the 15th, 2019 at 21 sites and GNSS-measurements were performed at 7 sites. All the sites are permanent sites where gravity had previously been measured except for one site close to Leirhnjúkur (site BF21, see Figure 6). Figure 4 shows the locations of the GNSS-sites; otherwise, the GNSS measurements are described in Chapter 4.
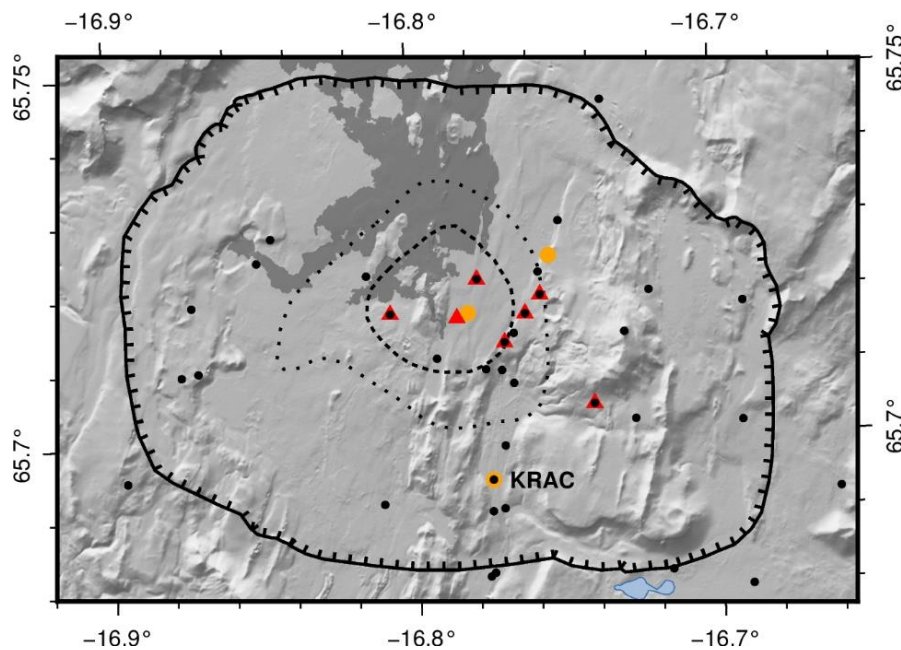
Figure 4. *GNSS-measurements in the Krafla area in November 2019. Orange filled circles denote continuously recording GNSS-stations; KRAC is a station established in 2011 while the other two were added in November 2019. Red filled triangles with black points denote older GNSS-stations (campaign sites) that were measured in the November survey, triangle without black is a new site measured, and black dots are old campaign GNSS-stations not measured. The ticked line indicates the Krafla caldera. The dashed line marks the area with clear inferred uplift in 2019, while the dotted line encircles the area with indication of uplift as seen by InSAR data.*

Gravity was measured in the 2019 campaign using the Scintrex CG5 gravimeter. A description of the measurement procedure and the processing of the data is found in a report by Magnússon (2016). The location of the gravity sites is shown in Figure 5 and the layout of the campaign in Figure 6. Gravity was measured at most of these permanent sites in Krafla in 2017 and 2018 by Portier et al. (2018) as a part of a bigger survey.

Table 1 gives an overview of the three gravity surveys from 2017, 2018 and from 2019: Name, coordinates, height above sea-level and gravity. Two names are given for the gravity sites. On one hand the name which has been used by ÍSOR through the years and on the other hand a new name invented and used by Portier et al. (2018). Absolute gravity was measured in 2017 and 2018 at station 200 in the northern part of the garage, to the north of the power plant (Portier et al., 2018).
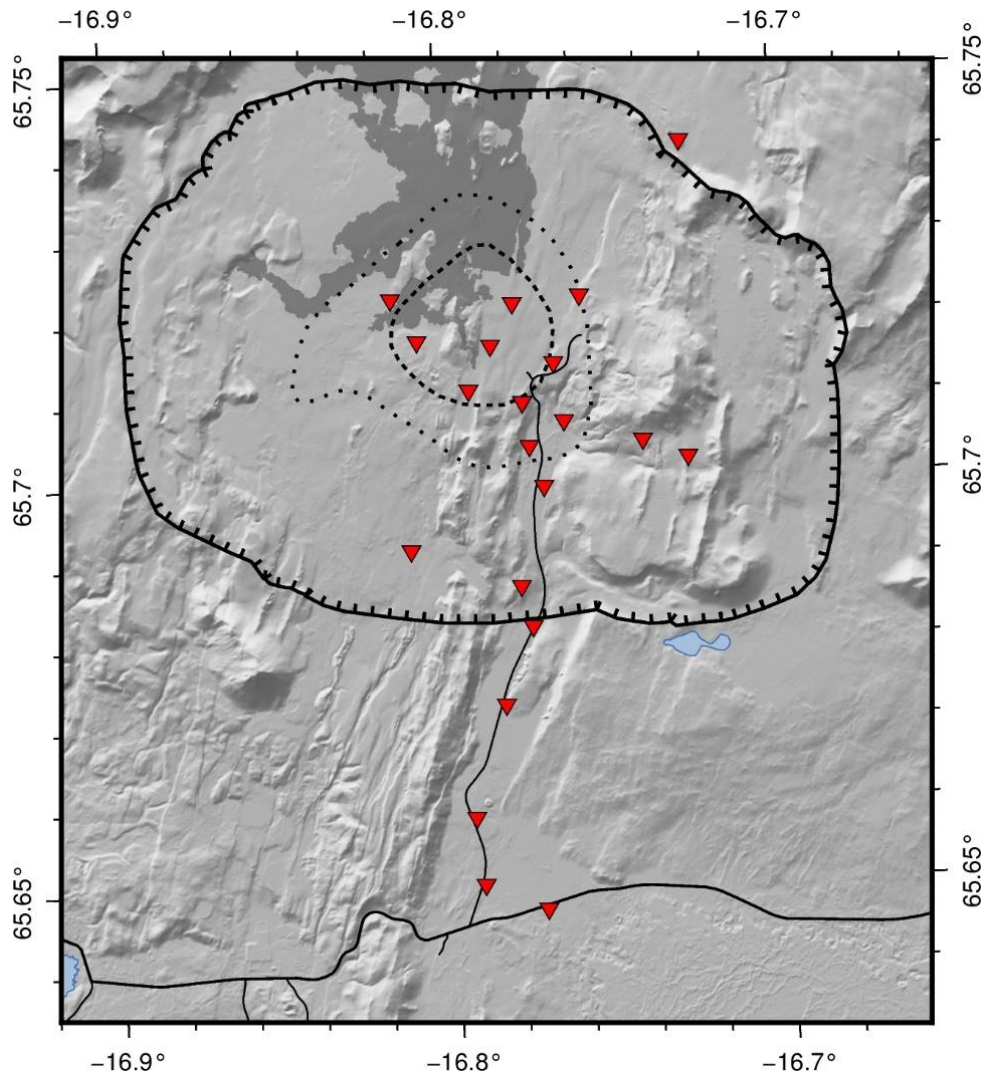
Figure 5. *Gravity measurements in the Krafla area, November 2019. Red, filled inverted triangles denote gravity stations. The ticked line indicates the Krafla caldera. The dashed line marks the area with clear uplift while the dotted line encircles the main uplift as seen by InSAR data. Solid, black lines are roads.*

The gravity values from the 2019 campaign in Table 1 are relative to a base station T517, the southernmost gravity site which is shown on Figure 5 and 6. All the gravity measurements were performed at permanent sites except for measurement BF21. There, a new permanent site was installed. Gravity values in Table 1 have not been corrected for different elevations between the surveys. On the other hand, the values were corrected for the influence of the sun and the moon, height of the gravimeter above the ground and drift.

Table 2 shows the elevation changes at the permanent sites from 2017 to 2018, and from 2018 to 2019, respectively, as calculated from InSAR data. These are relative to site T517. Furthermore, free-air gravity corrections due to the different elevation in 2018 and 2019, respectively, at the permanent sites are given as well as the gravity changes between 2018 and 2019 and finally the corresponding free-air corrected gravity changes from 2018 to 2019. Figure 7 shows the gravity changes between the 2018 and 2019 campaigns including the free-air correction.
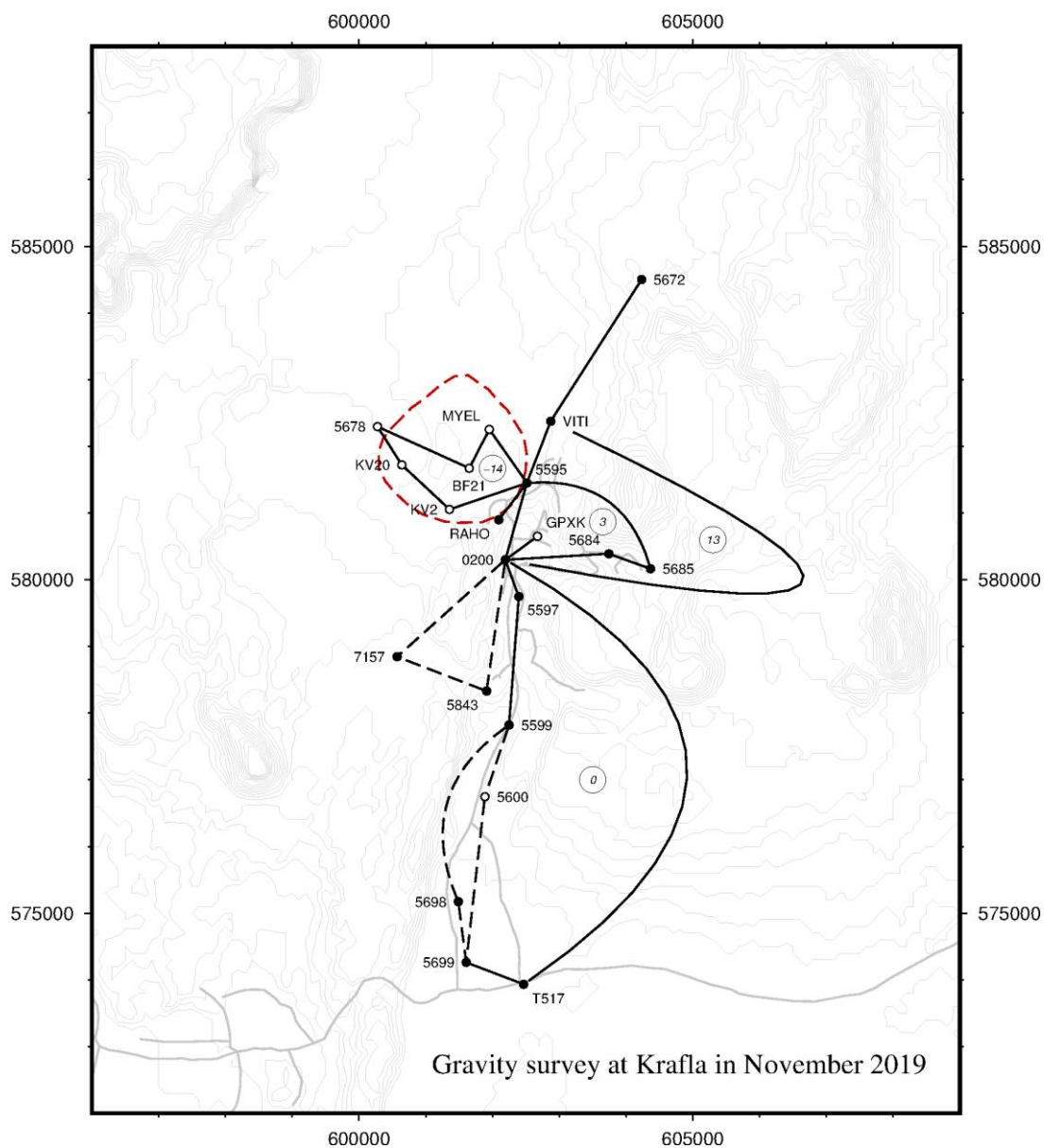
Figure 6. *Gravity measurements in the Krafla area, November 2019. Black filled circles are stations from the 200-series in Portier et al. (2018). Open circles are other stations, mostly old ones. BF21 close to Leirhnjúkur denotes the new permanent site. Continuous lines show interconnection between measurements back and forth while dashed lines those that were not measured back and forth. Red dashed line encircles the main uplift (see also Figure 4 and 5).*

Table 1. *Gravity measurements in the Krafla area from the 2017, 2018 and 2019 campaigns.*

Name used by ÍSOR	Name used by Portier et al. (2018)	Latitude (N)	Longitude (V)	Height a. sl. (m)	2017 Gravity (mGal) (Portier et al., 2018)	2018 Gravity (mGal) (Portier et al., 2018)	2019 Gravity (mGal) (ÍSOR)
200	200	65°42'14.8"	16°46'28.6"	460.00	53.009	53.018	53.036
201	201	65°38'42.0"	16°54'55.0"		82.505		
206	206	65°38'13.9"	16°48'33.4"		65.591	65.604	
207	207	65°38'25.4"	16°51'30.2"		73.361	73.393	
2313	205	65°38'40.9"	16°48'09.0"		66.961	66.972	
5595	219	65°42'51.5"	16°46'00.0"	551.62	36.287	36.301	36.310
5597	202	65°41'56.7"	16°46'14.2"	457.88	53.763	53.764	53.801
5599	208	65°40'54.8"	16°46'31.0"	394.62	66.776	66.786	66.805
5599A	212	65°40'53.0"	16°46'36.1"	394.75	66.744	66.753	
5600	203	65°40'20.5"	16°47'02.2"	389.59	66.469	66.485	66.517
5672	222	65°44'28.0"	16°43'36.8"	659.69	14.910	14.905	14.891
5678		65°43'21.4"	16°48'53.1"	520.51			44.029
5684	216	65°42'15.9"	16°44'26.9"	610.43	21.016	21.034	21.030
5685	217	65°42'07.9"	16°43'38.5"	626.75	18.750	18.762	18.764
5688	218	65°42'08.8"	16°46'36.4"	462.08	53.321	53.336	
5697	224	65°39'51.4"	16°47'33.5"	380.99	66.604	66.617	
5698	204	65°39'30.0"	16°47'37.8"	372.41	66.829	66.833	66.866
5699	211	65°39'00.6"	16°47'30.9"	361.27	67.103	67.108	67.121
5843	215	65°41'11.6"	16°46'55.9"	461.41	51.531	51.558	51.552
6123	210	65°39'00.0"	16°44'55.3"	359.13	67.132	67.137	
7157	221	65°41'29.7"	16°48'39.4"	471.55	51.372	51.397	51.407
24072	209	65°38'38.3"	16°40'12.3"	366.42	63.154	63.155	
BF11	213	65°38'42.7"	16°42'11.2"	366.02	63.423	63.429	
BF21		65°42'59.7"	16°47'07.1"	541.00			40.719
GPXK		65°42'25.6"	16°45'50.4"	460.00			50.671
KV2		65°42'40.1"	16°47'32.0"	530.07			40.643
KV20		65°43'02.4"	16°48'26.1"	537.74			39.051
MYEL		65°43'18.1"	16°46'41.9"	545.00			39.001
RAHO	220	65°42'34.2"	16°46'34.7"	558.00	32.605	32.632	32.625
T517	214	65°38'49.1"	16°46'24.6"	359.09	66.675	66.683	66.683
VITI	223	65°43'21.0"	16°45'29.5"	563.00	35.915	35.924	35.913

Table 2. *Elevation changes at the gravity sites in Krafla from 2017 to 2018, and from 2018 to 2019, respectively. Free-air correction and gravity changes between the 2018 and 2019 campaigns.*

Name ÍSOR	Elevation changes 2017-2018 (mm)	Elevation changes 2018-2019 (mm)	Free-Air Correction 2018-2019 (µGal)	Gravity changes 2018-2019 (µGal)	Free-air corrected gravity changes 2018-2019 (µGal)
200	-3	7	2	18	20
206	-2				
207	-5				
2313	-2				
5595	-3	5	2	9	11
5597	-2	5	1	37	38
5599	1	-1	0	19	19
5599A	1				
5600	0	-2	-1	32	31
5672	-1	0	0	-14	-14
5678	-2				
5684	-1	0	0	-4	-4
5685	-1	0	0	2	2
5688	-3				
5697	-1				
5698	-2	-2	-1	33	32
5699	-1	-1	0	13	13
5843	0	-3	-1	-6	-7
6123	2				
7157	-2	1	0	10	10
24072	0				
BF11	0				
BF21	-3				
GPXK	-4				
KRAC	-2				
KV2	-4				
KV20	-4				
MYEL	-2				
RAHO	-3	6	2	-7	-5
T517	1	1	0	0	0
VITI	-2	3	1	-11	-10
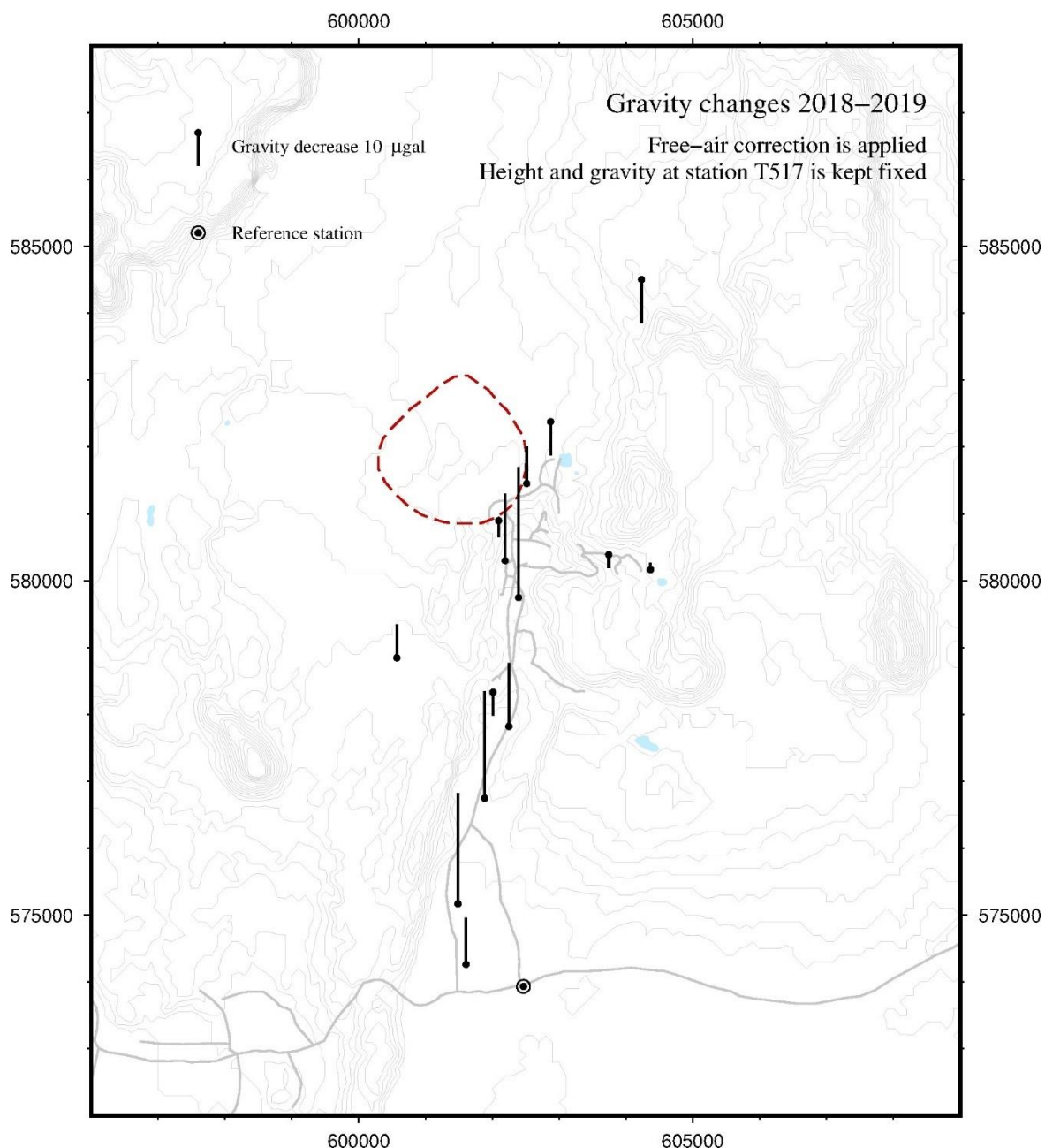
Figure 7. *Free-air corrected gravity changes from 2018 to 2019, relative to gravity site T517 (see Figure 6). Data have been corrected for elevation changes between 2018 and 2019 as shown Table 2. Red dashed line encircles the main uplift (see also Figure 4 and 5).*

Figure 7 shows the gravity changes from 2018 to 2019. Unfortunately, Portier et al. (2018) did not measure gravity in the 2017 and 2018 campaigns inside the main uplift area. ÍSOR's experience is that the mean uncertainty in similar surveys is 10-15 μGal. It is noteworthy, that the two northernmost sites show negative gravity changes while most of the others show a positive gravity change which varies between 10 and 38 μGal. The stations with positive gravity changes lie south of the power station in Krafla. It is not likely that these changes are affected by the processes that cause the inflation. Increase in groundwater level by 3 to 4 m with 20% porosity (or 6 to 8 m with 10% porosity) could make these changes. Assuming that

the inflation is due to a magmatic intrusion it is still so small that it is not detected yet as a gravity increase.

It should be stressed here that these series of gravity measurements are most important if the uplift continues, for a further understanding of the ongoing subsurface processes that might be causing the uplift. Furthermore, it should be noted that the measurements of the 2017 and 2018 campaigns do not cover the main uplift area well. However, as described above, in 2019 that area was measured for further monitoring.

4 GNSS observations and inferred ground deformation in relation to inflation at Krafla (CL, SL, FS, SH, HG)

4.1 Winter 2019 and Summer 2020 GNSS campaigns

Following GNSS measurements in summer 2018 in the Krafla area, an additional campaign was carried out 11-15 November 2019 in the Krafla caldera (Figure 8) to further study the inferred inflation of the area. Two new continuous sites were installed (LHNC and SPBC), and instrumented were set up on other 9 stations. One of these stations was new (LHSA). However, there were some issues with data from two sites (KMDC and KMDA). Data analyses have so far provided good results for 7 stations (there were some problems with the data file recorded by the receiver and/or the antenna used for KMDC and KMDA). GNSS instruments used for the survey were provided by the Institute of Earth Sciences (IES) (Receivers: Trimble 5700 and SEPT POLARX5; Antennas: Trimble Zephyr Geodetic-TRM41249.00- and navXperience 3G+C for the new continuous stations).

Figure 8. *Map of measured GNSS station in Krafla in November 2019, in white. Green label is for the recently installed continuous GNSS stations: LHNC and SPBC, and the former continuous KRAC station, installed in 2011.*

In July 2020 a GNSS survey was carried out with over 60 stations measured in Krafla, Bjarnarflag and Þeistareykir areas. We only report here on the Krafla and Bjarnarflag results (Figure 9). GNSS instruments used for the survey were provided by the Institute of Earth Sciences (IES): (Receivers: Trimble 5700, R7, NETR9 and SEPT POLARX5; Antennas: Trimble Zephyr Geodetic (TRM41249.00), Trimble Zephyr Geodetic II (TRM57971.00), and navXperience 3G+C).

Figure 9. *Map of measured GNSS network in Krafla (upper) and Bjarnarflag area (below). Green label is for the continuous GNSS station.*

For both the November 2019 and July 2020 campaigns, each GNSS station was measured around 48 hours, sampling data every 15 seconds. The data were analyzed at University of Iceland using the GAMIT/GLOBK analysis software (Herring et al., 2010). Site positions were evaluated in the ITRF2014 reference frame using over 100 worldwide reference stations. The data were corrected for ocean tidal loading using the FES2004 model (Lyard et al., 2006). The time-series were corrected for the velocity of stable Eurasian plate using the GAMIT/GLOBK software, based on the ITRF2008 plate motion model (Altamimi et al., 2012).

In addition to the campaign measurements described above, continuous GNSS stations, KRAC, SPBC and LHNC (Krafla caldera), BJAC and MYVA (Bjarnarflag) are collecting data all the year.

4.2 Time series

4.2.1 Continuous GNSS stations

There are currently 5 continuously recording GNSS stations in the Krafla and Bjarnarflag area (Figure 4 shows the three of them within the Krafla caldera). Four of them are operated by the IES in collaboration with Landsvirkjun: KRAC, installed in 2011 near the Krafla power plant and BJAC installed in 2012 south of Námafjall. The two stations installed in November 2019: LHNC, east of Leirhnjúkur and SPBC north of the Víti crater. The MYVA station was installed in 2006 in Reykjahlíð by Christof Volksen from the Bavarian Academy of Sciences and Humanities and is operated by the Land Survey of Iceland. The data are transferred daily and analysed at the computer facility at University of Iceland. Data is analysed with different software: GAMIT/GLOBK and GIPSY.

The continuous KRAC site is clearly influenced by the inflation episode beginning in the middle of 2018. The data have been analysed with different software giving times series of displacement of the site in the North, East and Up components in millimetres (Figures 10 and 11). The time series (processed with GYPSY and GAMIT/GLOBK) are detrended in such a manner that constant, annual and semi-annual variations are removed from the time series. Therefore, they only show unusual deformation. The results from the two processing strategies are in good agreement, but some differences remain at the mm-level. Both show unusual displacement beginning in middle of 2018, witnessed as southward movement that at present amounts to about 18 mm. In a simple deformation model consisting of a point source of pressure within elastic half-space, then horizontal displacement will be in direction pointing directly away from the source. Southward displacement at KRAC is in an agreement of pressure increase in the crust to the north of the station. The inferred temporal history of southward displacement is somewhat different according to the two softwares used to analyze the data. The time series in Figure 10 show clearly increased southward displacement rate in June 2018 and later and changes in late 2019 whereas the time series in Figure 11 has slightly more uniform rate of southward movements.
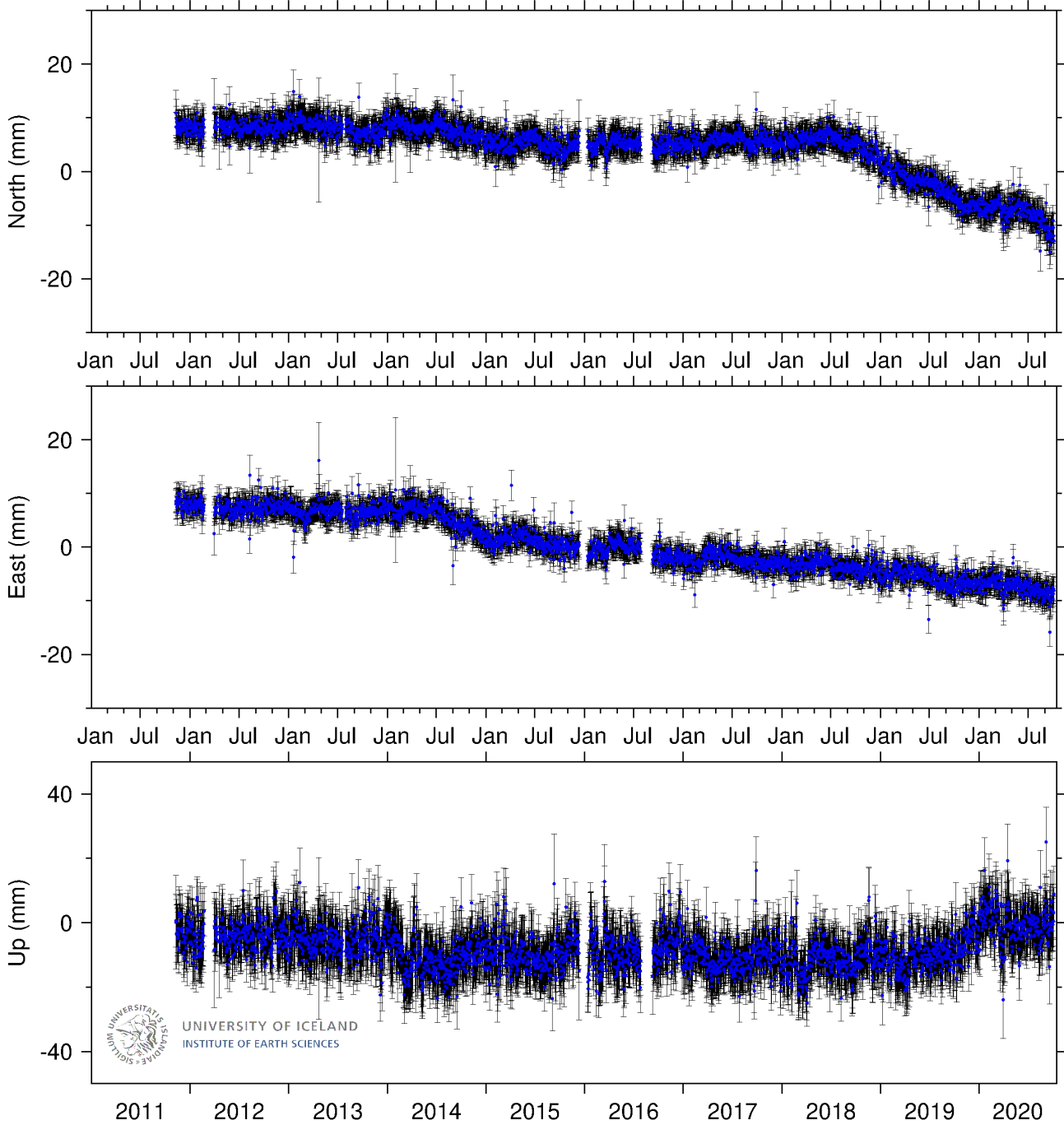
Figure 10. *GNSS time series for KRAC GNSS station at Krafla as analysed by Sigrún Hreinsdóttir. Displacements are detrended using constant velocity rates of 21.3mm/yr -5.6mm/yr and 3.1 mm/yr for north, east and up, respectively, in the ITRF08 and annual and semi-annual terms estimated using time series analysis.*
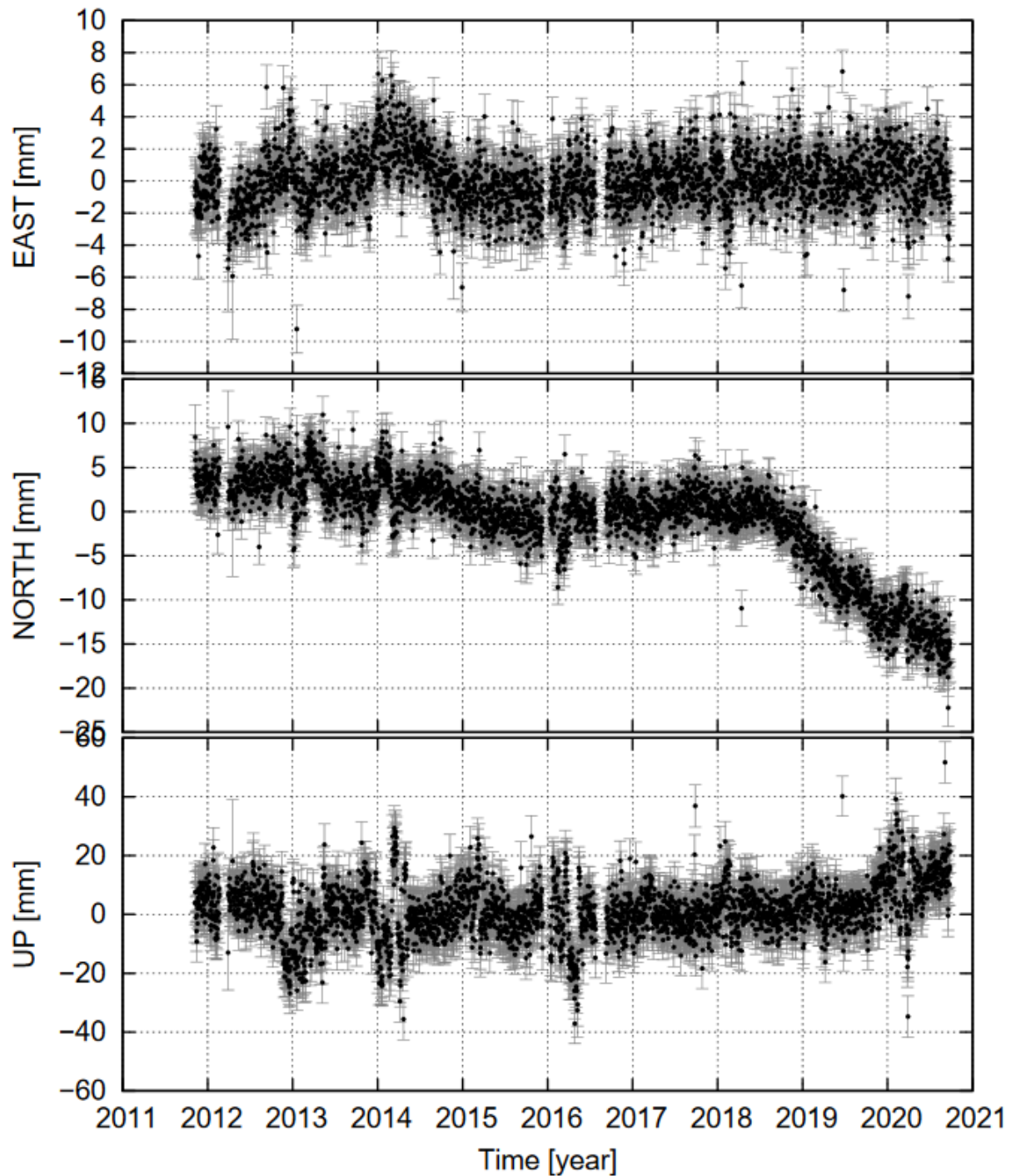
Figure 11. *GNSS time series for KRAC GNSS station at Krafla as analysed by Halldór Geirsson. Displacements are detrended using constant velocity rates in the ITRF08 and annual and semi-annual terms estimated using time series analysis.*

Time series for the new continuous stations in the Krafla area installed in November 2019, LHNC and SPBC, are presented in Figures 12 and 13, respectively. For these stations, the time series are detrended for linear variations only. At present, the time series for these two stations are still too short to estimate their seasonal signal. In addition, for the LHNC time series a part of the data has been removed due to major perturbations during the time span not shown. The

most probable cause is presence of a thick snow cover; the station's antenna was buried completely by snow. Although short, these time series are broadly consistent with about stable velocities since their installation in November 2019.
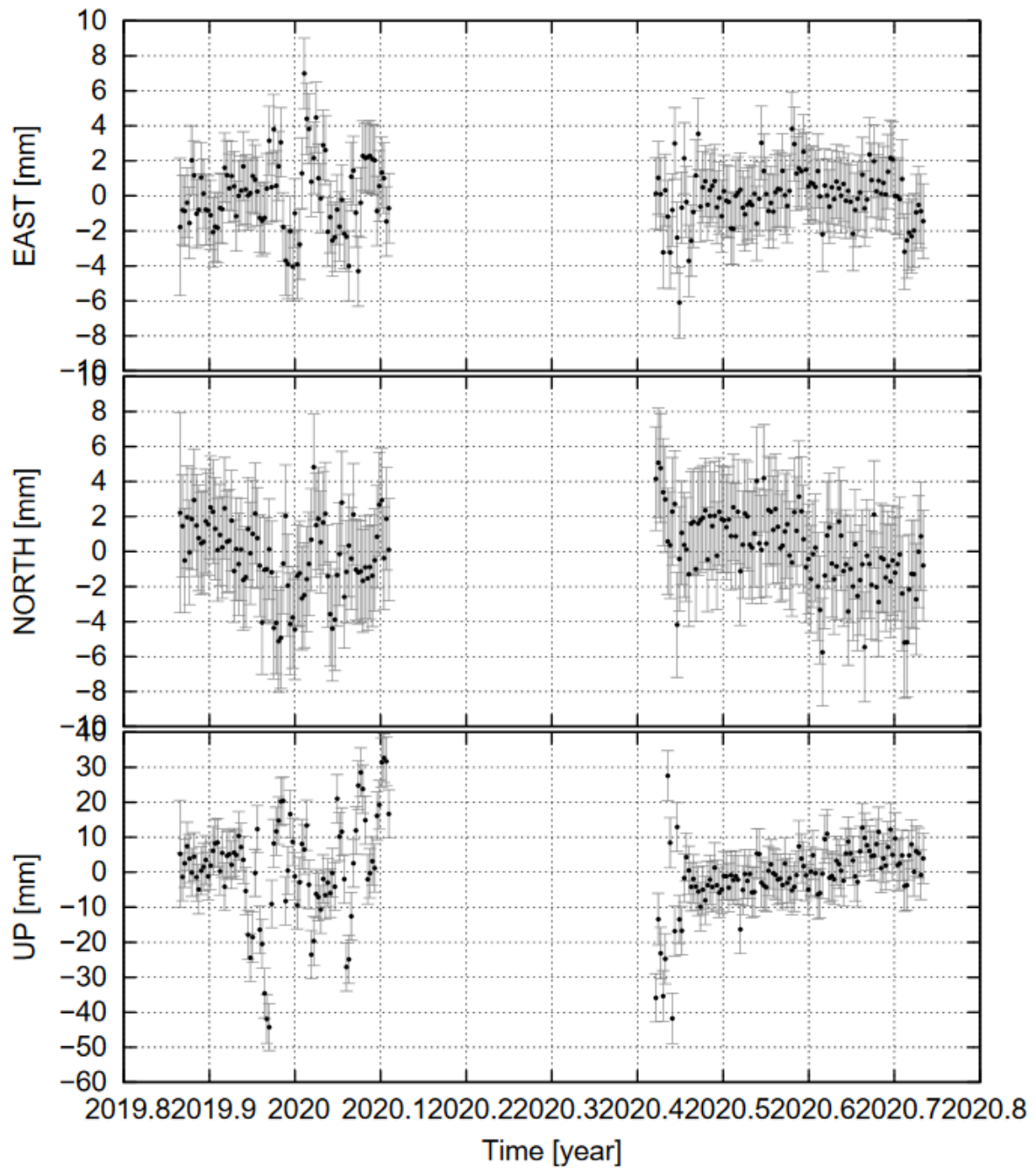
Figure 12. *GNSS time series for LHNC station in Krafla. Displacements are detrended for linear variations in the ITRF2014. Data analysis by Halldór Geirsson.*
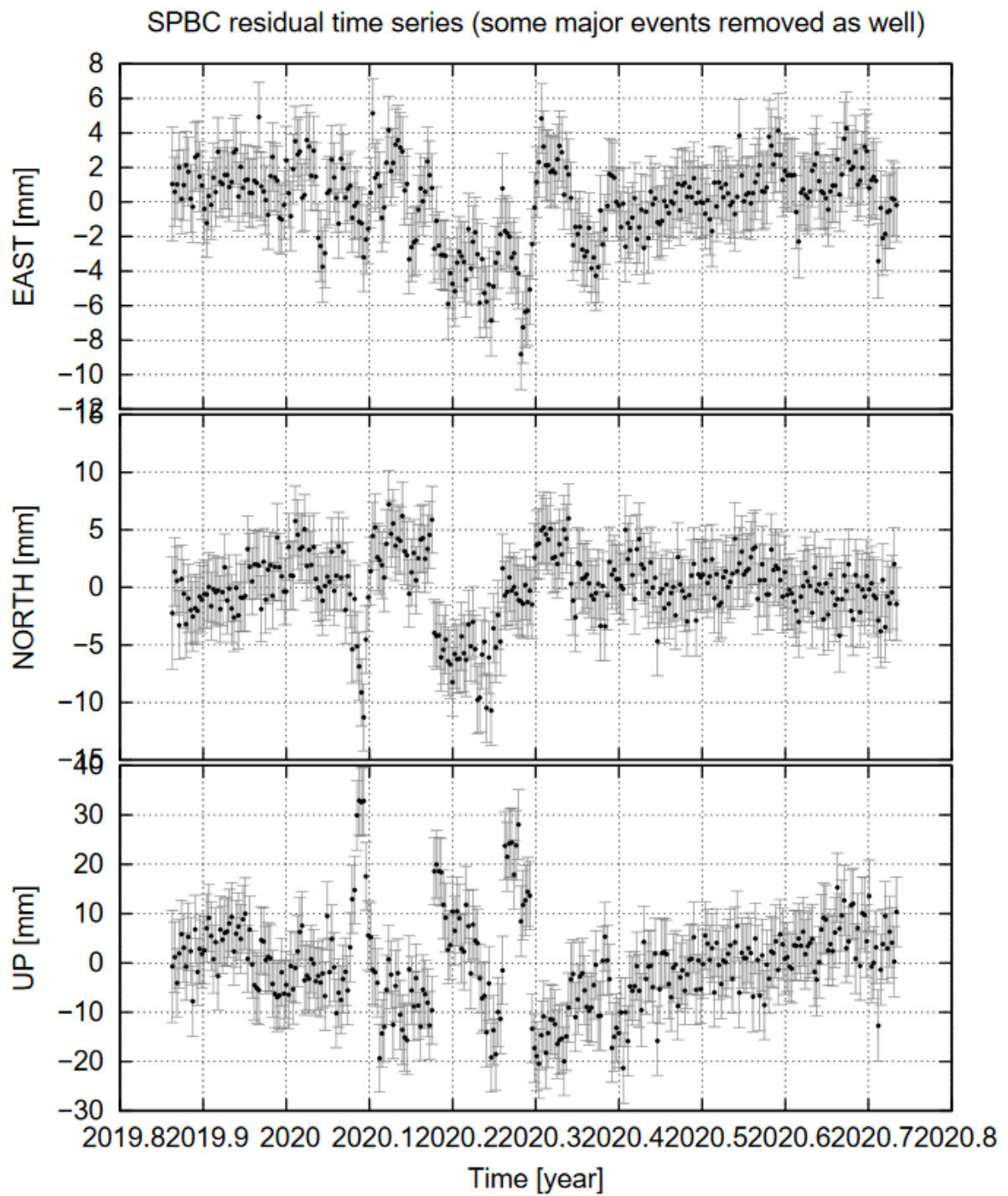
Figure 13. *GNSS time series for SPBC station in Krafla. Displacements are detrended for linear variations in the ITRF2014. Data analysis by Halldór Geirsson.*

4.2.2 Campaign GNSS stations

We here show times series of some selected campaign GNSS stations that can give further indications of the temporal history of deformation (Figure 14). The time series were then analyzed with Tsview software (Herring an McClusky, 2009). One of longest time series in the Krafla caldera is at VITI station, located north the Viti crater. The station has been measured yearly since 2012 (Figure 15). The inferred north movement is regular, but clear changes occur in the east and up components where the station moves along a different trend after 2018. Station L684 (Figure 15) shows a change in east component after 2018. The last measurement (this year) at station KMDA shows clearly a higher elevation than before (Figure 16, upper), whereas such change is not evident at the nearby KMDB station (Figure 16, lower). These stations are not located in good bedrock and some variation may be due to site instability.
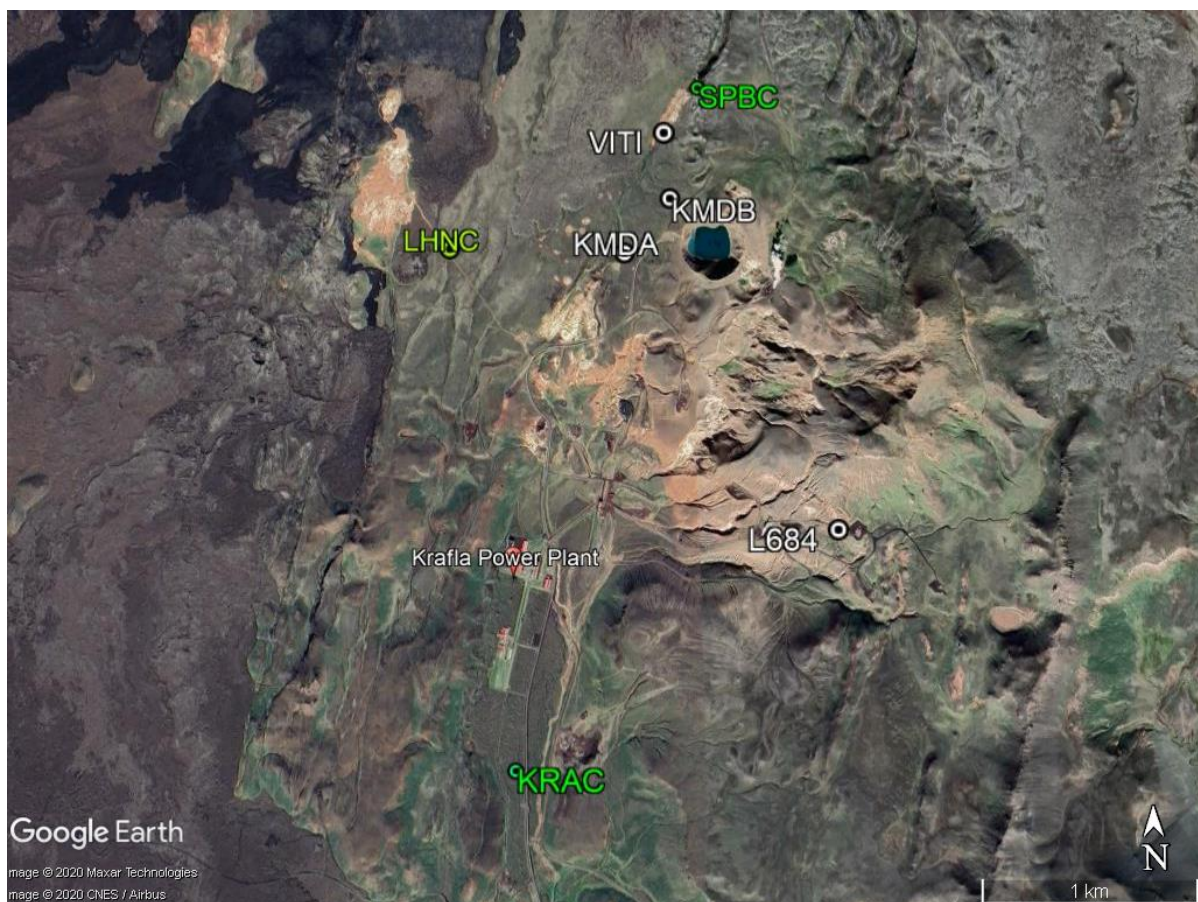
Figure 14. *Location of selected stations time series shown in Figures 10 and 11. Campaign GNSS stations VITI, L684, KMDA, and KMDB (white). Time series from continuous GNSS KRAC, SPBC and LHNC (green) are shown in Figures 10-13.*
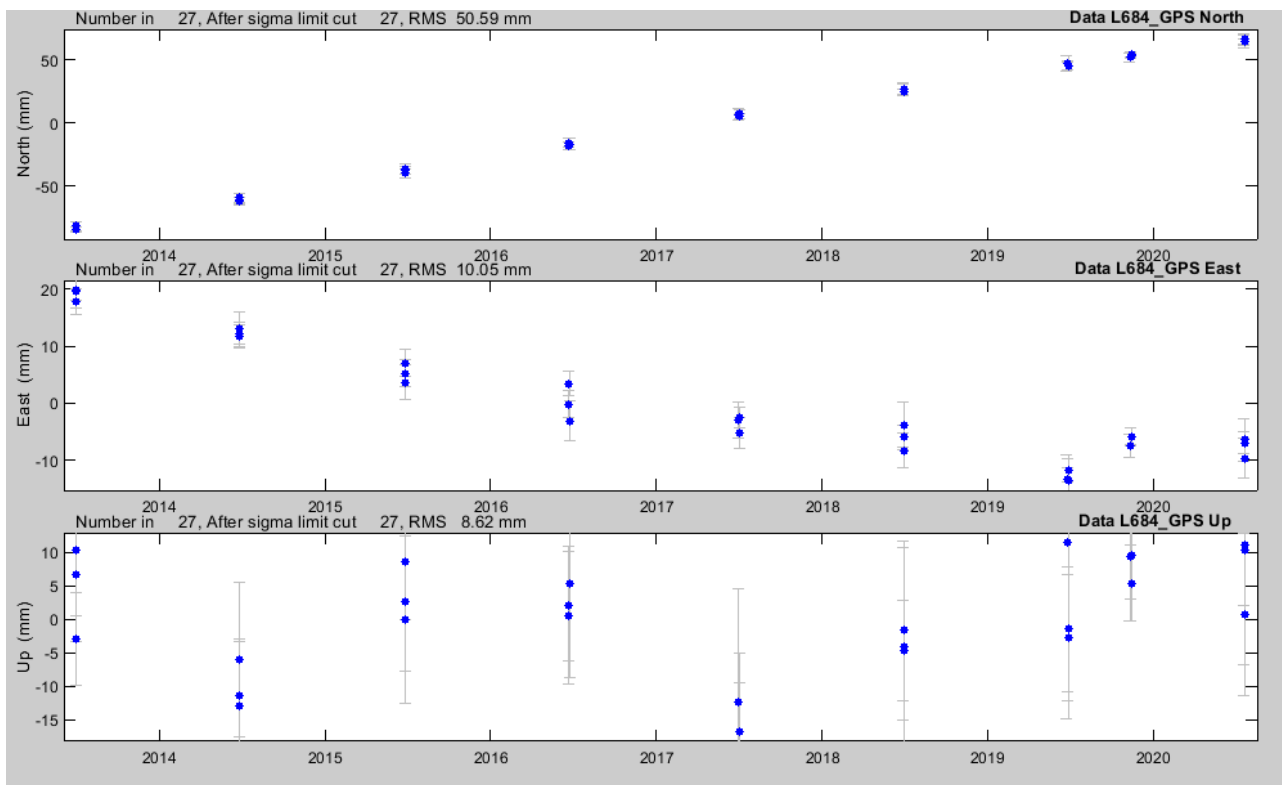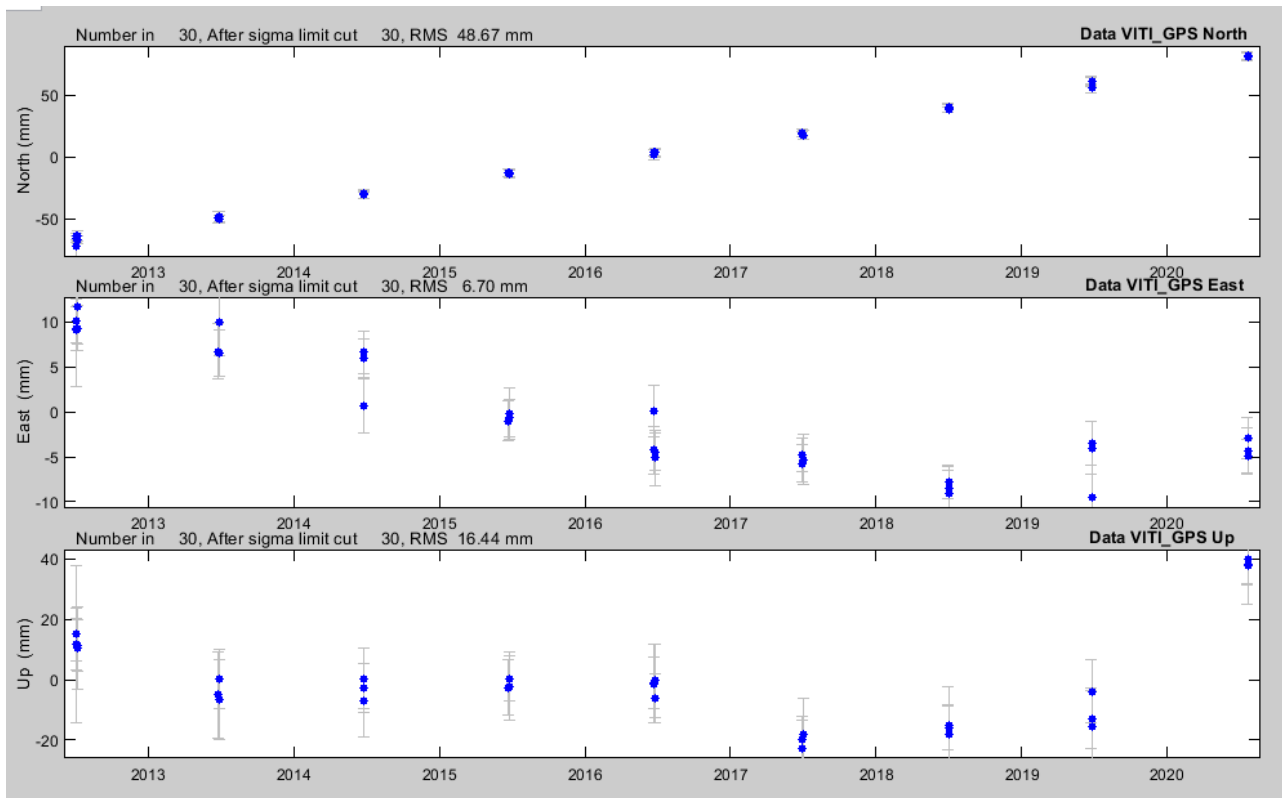
Figure 15. *Time series for VITI (upper part) and L684 (lower part) stations. Displacements are in the ITRF08 reference frame. GNSS solutions (blue dots) and uncertainties (vertical lines). Data were typically collected for 2-3 consequent days each year, and data from each day then analyzed separately (resulting in 2-3 estimates reflecting uncertainty.*
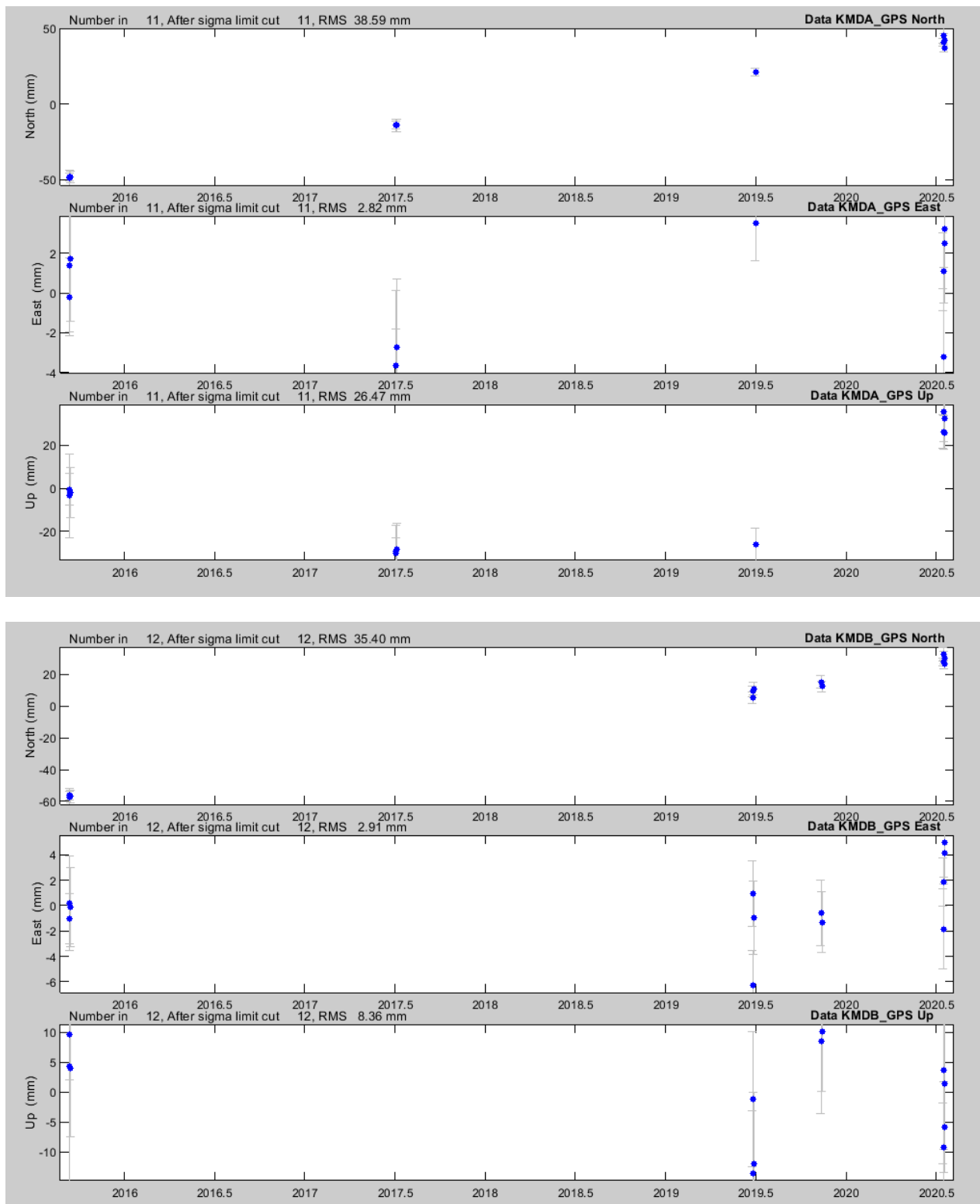
**Figure 16.** *Time series for KMDA (upper part) and KMDB (lower part) stations. Displacements in the ITRF08. GNSS solutions (blue dots) and uncertainties (vertical lines).*

Overall, the time series of displacement at the campaign GNSS sites show changes that support well the results from the continuous GNSS sites, indicating an inflation period at Krafla after middle of 2018.

4.3 Velocity fields

The previous chapter with time series of displacement at GNSS sites gives an indication of the temporal evolution of deformation. The GNSS can also give a more complete indication of the spatial changes, complementing the InSAR observations. For this purpose, we evaluate ground surface velocity fields based on the GNSS data collected in different campaigns. We can use the time-series to estimate the average velocity at the GNSS stations for different time periods. Velocities were initially estimated in the ITRF08 reference frame. Then, using the ITRF2008 plate motion model (Altamimi et al., 2012), they are converted into velocities relative to the Eurasian plate. From these it is possible to derive three-dimensional displacement velocities for all the stations that have been measured at least two time during the chosen time interval.

We initially evaluate the velocity field for the 2015-2018 pre-inflation time period (Figure 17) and then, the velocity field for the inflation period, 2018-2020 (Figures 18 and 19). Overall horizontal velocities show westward motion of about 10 mm/yr (95% confidence interval). Due to the location of the study area near the central axis of the plate boundary (at the central axis half of the plate velocity should be observed, as the reference is the stable Eurasian plate). The pattern of vertical velocities is different in the two periods. In the 2015-2018, the velocity field show an overall subsidence in the centre of the caldera and at Bjarnarflag, while in 2018-2020 (Figure 19) the overall pattern indicates inflation in the centre of the caldera, with some exceptions. L603 station (Bjarnarflag area, along the main road) shows a strong vertical signal (Figure 19). Considering the nearby pattern, we suspect some problems with the receiver or the antenna collecting the data at this site.
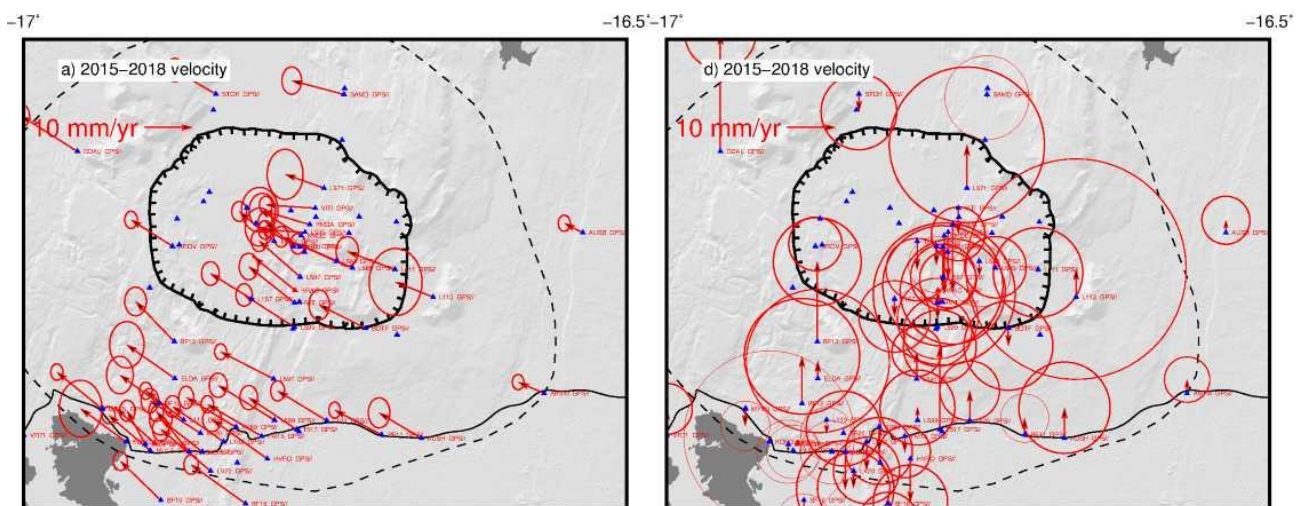
Figure 17. *2015-2018 horizontal (left) and vertical (right) GNSS velocities relative to the stable Eurasian plate, in the Krafla and Bjarnarflag areas. Blue triangles show the campaign GNSS station, while the red ones show the continuous station. Ellipses indicate velocity uncertainties.*
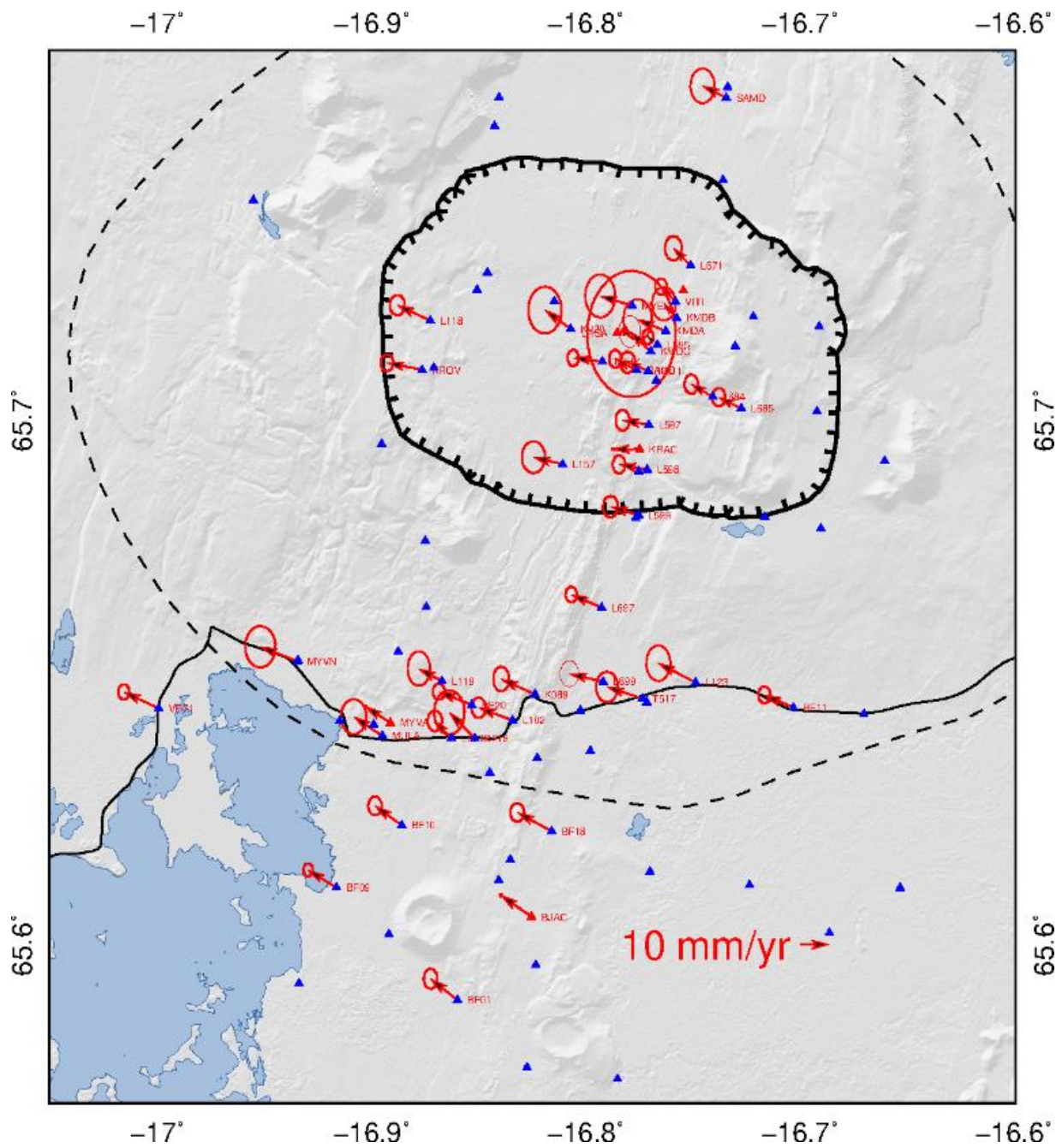
Figure 18. *2018-2020 horizontal GNSS velocities relative to the stable Eurasian plate in the Krafla and Bjarnarflag area. Blue triangles are campaign GNSS station, and red triangles continuous stations.*
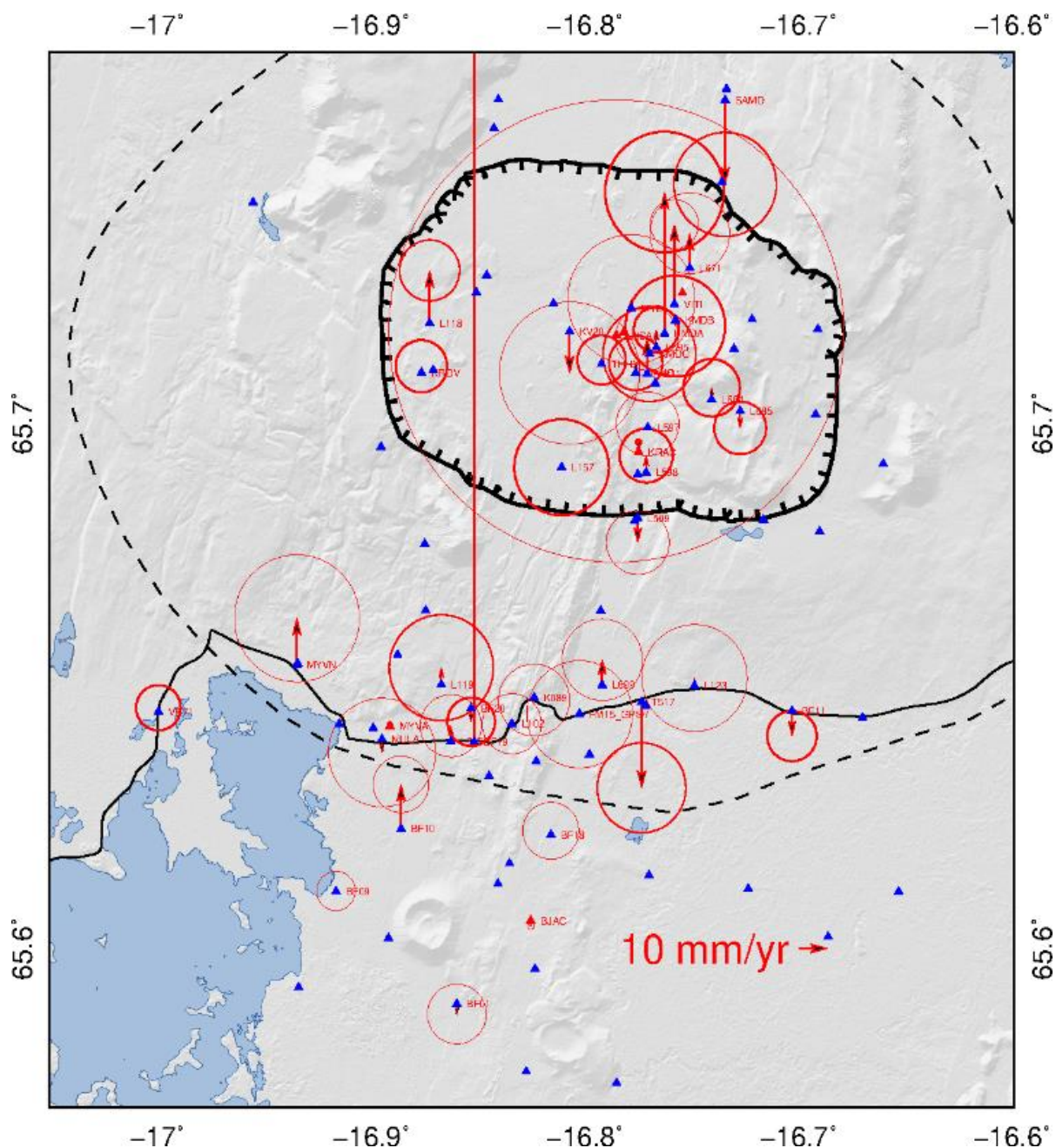
Figure 19. *2018-2020 vertical GNSS velocities relative to the stable Eurasian plate in the Krafla and Bjarnarflag area. Blue triangles are campaign GNSS station, and red triangles continuous stations.*

In order to make best use of the available data and investigate the change of the deformation pattern with respect to the time prior to the inflation, we consider now the difference in the velocity fields for the pre-inflation period (2015-2018) and the inflation period (2018-2020). This is the same strategy as for observing differences in the InSAR observations.

The difference in velocity between the inflation and the pre-inflation period is shown in Figures 20 and 21. These velocity differences provide a convenient way to isolate the signal related to the inflation, assuming other processes that were active in the pre-inflation period 2015-2018 continue in the following period. The horizontal velocity difference shows a general

movement away from the centre of the caldera. The largest velocities observed at KMDB, L598 and L118 are considered unrealistic and erroneous as if, we compare them with the nearest stations, they deviate from pattern observed at nearby stations, considering such short distance between the station. The reason for such an error can be site instability, antenna set up errors, or may relate to the analysis of the data. Similarly, large vertical velocities that deviate from values inferred at nearby stations (VITI, BF-10, MYVN) may be erroneous.

Overall, the GNNS observations as presented here agree well with the InSAR results.
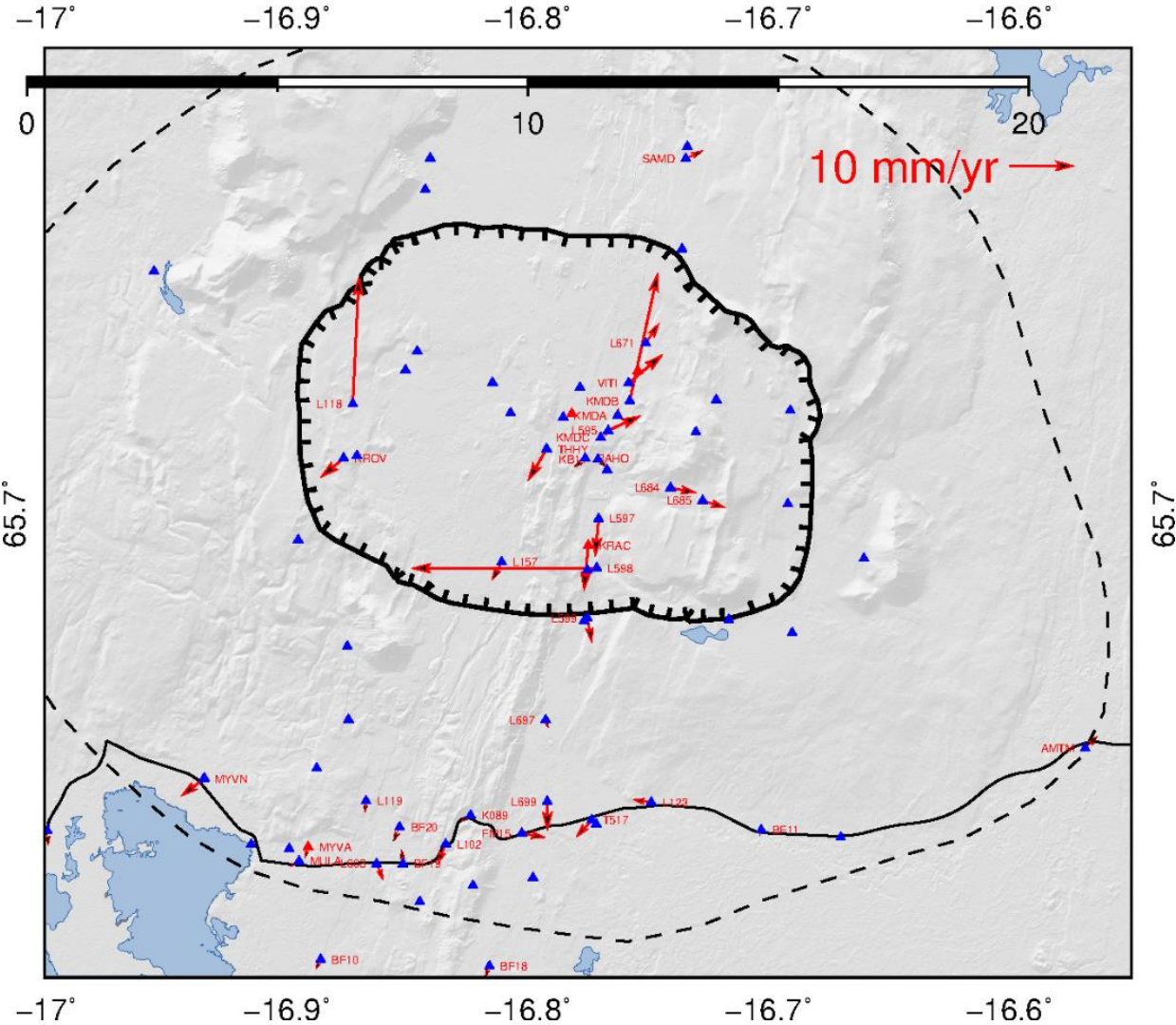
Figure 20. *Horizontal velocity difference (2018-2020 and 2015-2018), without uncertainties.*
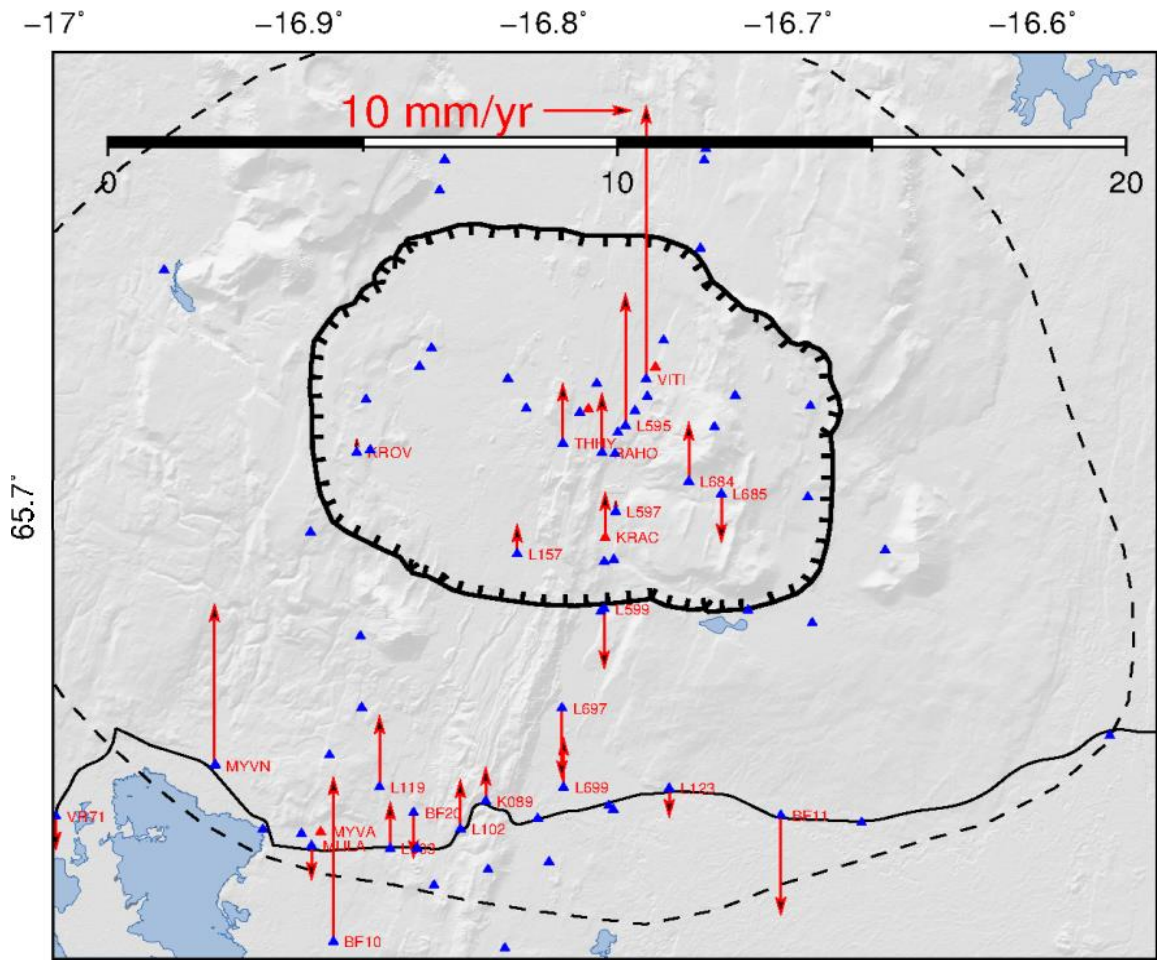
Figure 21. *Vertical velocity difference (2018-2020 and 2015-2018), without uncertainties.*

4.4 Modelling

The three-dimensional velocity difference field (2018-2020 with respect to 2015-2018; Figures 20 and 21) have been used to model the deformation at Krafla. In the following modelling, we use the GNSS stations that have a complete record from 2015 to 2020 (Figure 22) and similar line-of-sight (LOS) velocity difference fields from three InSAR satellite tracks, T9, T147 and T111 (Figure 1). We employ the open-source Geodetic Bayesian Inversion Software (GBIS, Bagnardi and Hooper, 2018), which allows to perform a joint inversion of GNSS and InSAR data to estimate deformation source parameters with a Bayesian approach. We here assume that deformation is caused by a spherical source of pressure within a uniform elastic half-space, a Mogi source (Mogi, 1958). The modelling procedures estimates then the horizontal location and depth of the source and volume change associated with it.

Figure 22. *GNSS stations with a complete record employed for the modelling of deformation. Shown as a yellow balloon is the inferred best-fitting location of a geodetic source fitting the data (see later in the chapter).*

The Bayesian approach for inverting the geodetic data finds probability density functions for each of the model parameters (Figure 23), and therefore a good estimate of model parameter uncertainties, considering the data and their uncertainties, and the assumptions inherent in the model approach. The results are presented below in Figure 23 and Table 3. The best-fitting horizontal location is shown in Figure 22 as yellow balloon. The modelling procedure estimates a depth ~ 2.5 km (2.2–3.0 km, 95% confidence interval) and a volume change $4.3 \cdot 10^5$ m³ (ranging from 3.9–$6.4 \cdot 10^5$ m³). Also, the resulting comparison between the velocity data and the estimation are in broad agreement. Figure 24 shows horizontal displacements; the black arrow (data) and red (estimation) moves away from an area indicated by the black star which is the inferred source location.
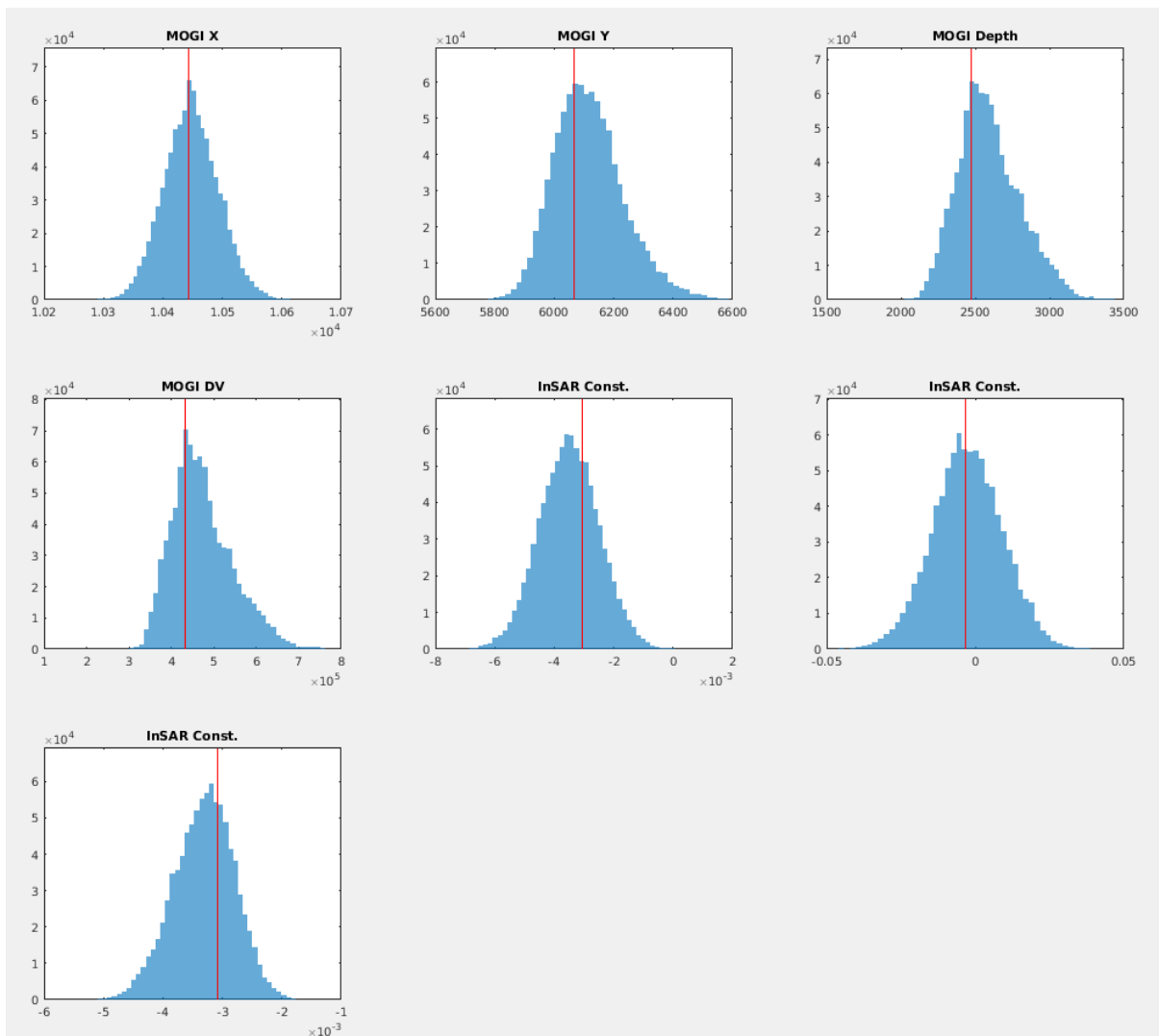
Figure 23. *Inferred probability density functions for geodetic model parameters. Source location (X and Y), source depth and volume change (DV). The input InSAR LOS velocity observations in each track are relative to an arbitrary reference. Therefore, three offset parameters (one for each of the InSAR satellite tracks used) are solved for in the modelling approach to take this into consideration.*

Table 3 presents a summary of the GBIS inversion results. In the first column, there are the model parameters, followed by the optimal, mean, median values. The last two columns show indicate the inferred 95% confidence range of model parameter as estimated in the process.

Table 3. *Results from GBIS inversion of 2018-2020 and 2015-2018 difference velocity fields from GNSS and INSAR. X and Y (modelling coordinate system) and depth in meters. Volume in m³. InSAR constants (three last lines) are parameters related to offset of InSAR velocity fields (considering their relative nature).*

MODEL PARAM.	OPTIMAL	MEAN	Median	2.5%	97.5%
MOGI X	10442.4	10447.9	10447.1	10359.5	10540.4
MOGI Y	6066.13	6117.34	6107.65	5917.22	6378.48
MOGI Depth	2469.57	2593.95	2572.31	2235.34	3051.42
MOGI DV	431433	473107	462713	358954	636838
InSAR Const.	-0.00307773	-0.00349349	-0.00349354	-0.00546395	-0.00152705
InSAR Const.	-0.00321247	-0.0026277	-0.00274487	-0.0258436	-0.0202258
InSAR Const.	-0.00307084	-0.00330948	-0.0032842	-0.00436054	-0.00236676

Figures 24 and 25 show a comparison of observed and predicted data according to the model. The observed signal is small, and some deviations of observations from predicted data according to a best fit model are evident. Nevertheless, the probability density functions for each parameter are well constrained. Figure 26 shows so-called convergence plot (for each model parameter). These plots indicate that after a so-called burn-in period (initial iteration search for parameter value with the approach used) the parameters are well constrained and lie within a certain parameter value range.
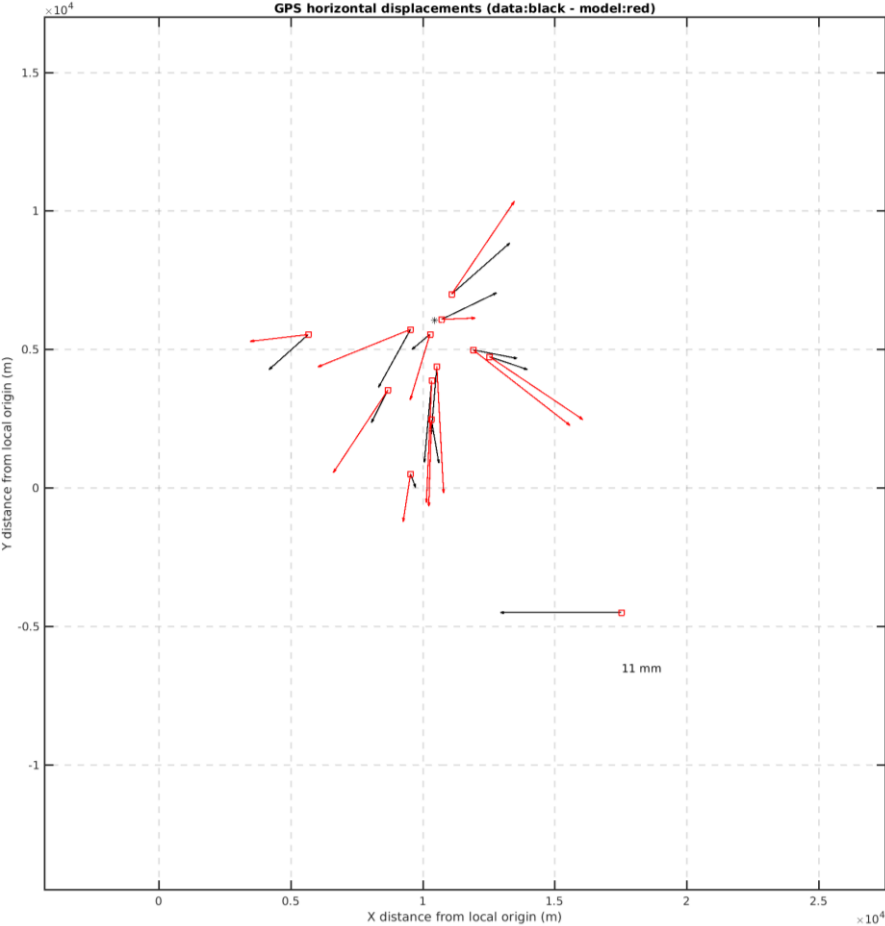
Figure 24. *Comparison between GNSS horizonal data and predictions of a best fitting model.*
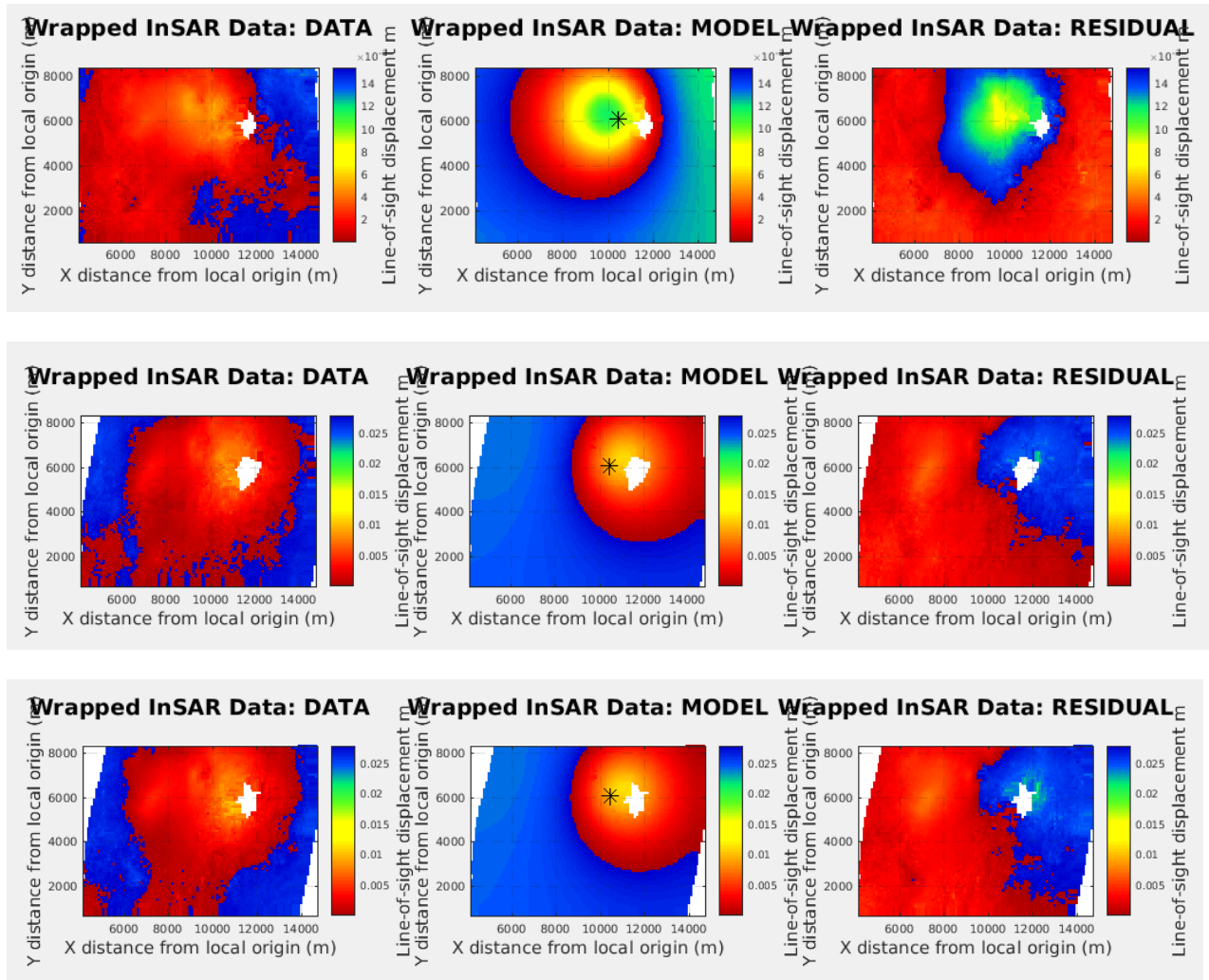
Figure 25. *InSAR data (panel on the left), best fit model (middle panel) and residuals (on the right) for InSAR tracks T147, T111 and T9, respectively. Local origin is an arbitrary reference location used when carrying out the modelling. Wrapped InSAR data refers to original phase change as evaluated in InSAR processing (considering length change is measured with the satellite signal wave).*
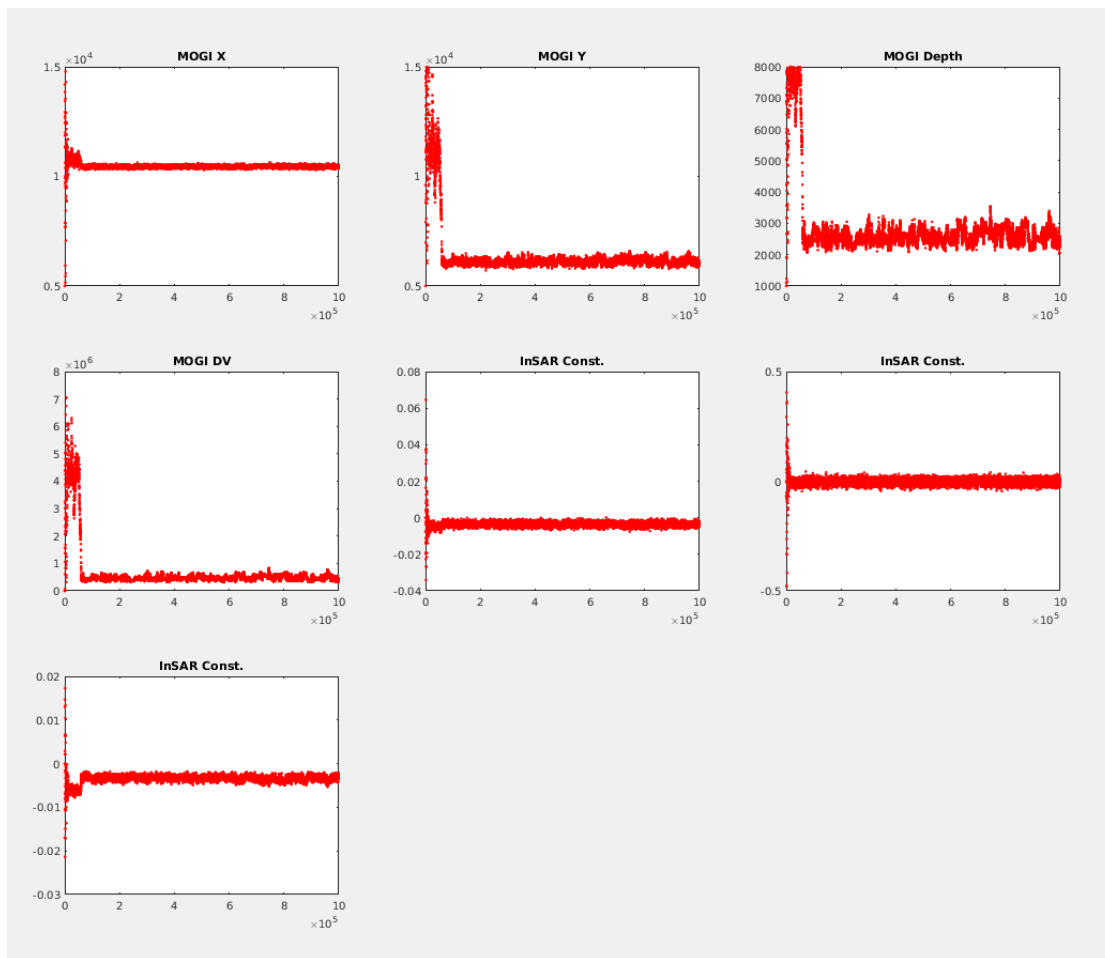
Figure 26. *Convergence plots for the Bayesian inversion approach. One million models were tested in the process as carried out. After a burn-in period of approximately 100.000 iterations, the model parameters remain relatively stable. Y-axis shows the inferred parameter value, and the X-axis shows iteration number.*

5 Seismic release (KÁ)

To investigate possible changes in the pattern of seismic release, only changes in seismic activity and moment rates for the whole Krafla area were investigated at this stage. The seismic activity in Krafla varies from year to year and during the time we have had the present seismic network (from late 2016 until now) the number of events per year have been between 5000 and 8500 events located per year (Blanck et al., 2020). The local magnitude estimate is considered quite reliable and for period from 2013 to now and magnitude estimate of all events is the same. Furthermore, the seismic network has not changed since late 2016 until now and there have not been changes in the procedure of location of events (e.g. velocity models) this time. The dataset is therefore internally consistent. The formula we use to estimate the moment release is by Hanks and Kanamori (1979).

The seismic rate increases slightly from 2013 to late 2016 as the seismic network was improved (Figure 27, left) and picks up more events. In the beginning of 2017, there is an increase and from the middle of 2017 until middle of 2019 the rate is rather constant. The rate decreases in

middle of July 2019 and increases again early 2020 (Figure 27, right) and reaches similar rate as before middle of 2019.

The moment release from 2013 to 2020 is shown on the left part of Figure 28. The large jump in December 2015 is due to an event of 2.96 Ml that is the far largest event recorded by the present network in Krafla. The rate of moment release increases in 2019 (Figure 28) and again in the beginning of 2020.

Figure 29 shows a weak decrease in the rate of cumulative number of events in the middle of 2018. Similar change in moment release seems to prevail but is not very clear. This time is approximately the start of the uplift in Krafla. In the middle of July 2019 there is a very clear change in the pattern of release. Minor changes in deformation in the time series of the continuous recording at station KRAC (Figures 10 and 11) are observed at this time. Then, in the beginning of 2020 cumulative rate of number of events increases and the moment release increases drastically. This is also simultaneous with changes that can be seen in Figures 10 and 11.
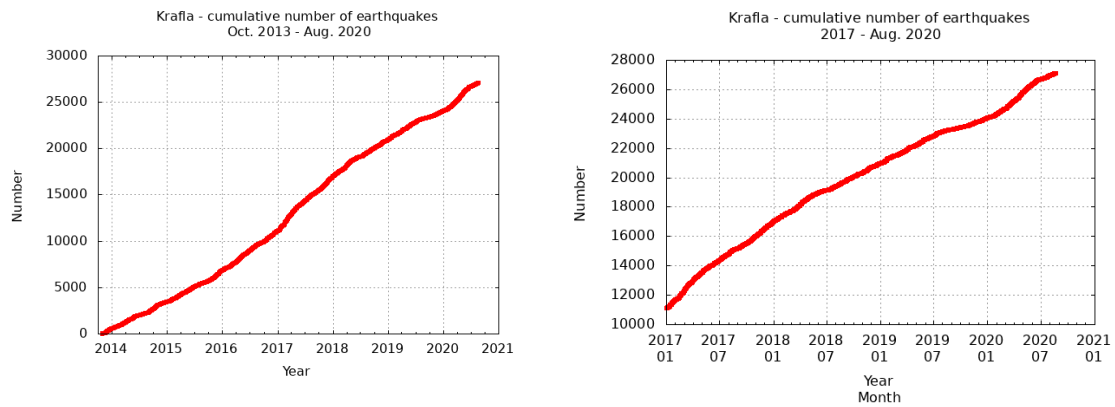

Figure 27. *Left is the cumulative number of events from 2013 to 2020 and right is the cumulative number of events 2017 to August 2020.*
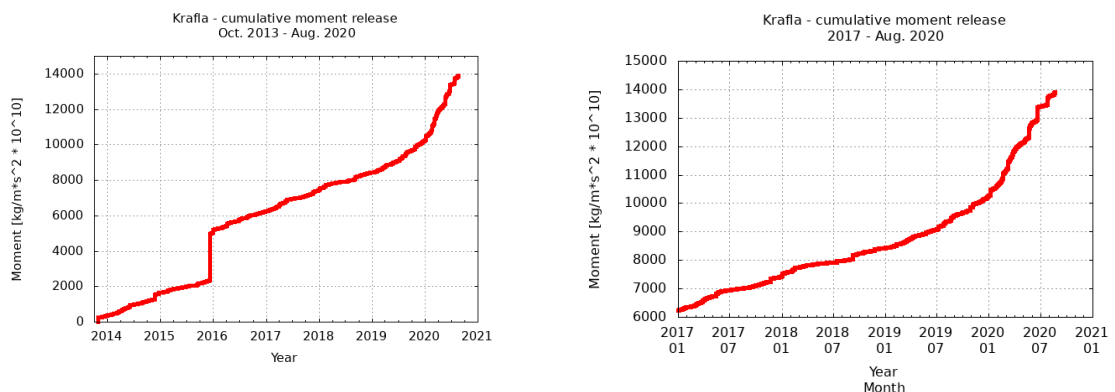
Figure 28. *Left is the cumulative moment release from 2013 to 2020 and right is the cumulative moment release 2017 to August 2020.*
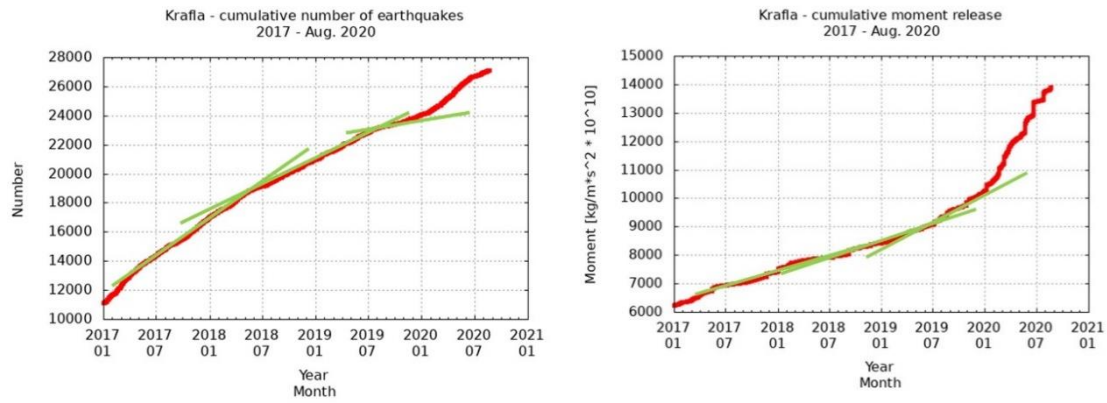
Figure 29. *Left is cumulative number of earthquakes in 2017 to 2020 and right is cumulative moment release for the same period. The green lines are linear approximations of the trends.*

In 2018 there is a slight increase in rate of moment release and as mentioned above, while the cumulative rate is decreased. This trend increases drastically after middle 2019. The change in the seismic release pattern shows that earthquakes become fewer but larger. Early in 2020 the cumulative rate of number of events increases such that the rate in the middle of the year is similar as in middle of 2018 to middle of 2019 but moment rate has increased significantly.

This can be interpreted as the crust is becoming stronger and consequently the energy is released in fewer and larger earthquakes. Simultaneously, there must be increased energy input that can be attributed to a magma intrusion or increased pressure in a magma chamber or other volume. It is natural that the local stress field changes when surface subsidence changes to uplift. Investigation of this demands a precise analysis of location of events and the character of seismic events together with analysis of the displacements observations and the deformation field that can be related to that as well as changes in gravity.

6 Interpretation and comparison with other data sets (FS, GPH and KÁ)

The geodetic data show changes in ground deformation pattern since middle 2018. When compared to ground velocity fields prior to 2018, an additional source of inflation is evident (Figure 30). Such inflation signifies increased pressure at depth in the Krafla caldera. Interpretation of the difference velocity fields suggests volume increase of about 0.5 million cubicmeters over two years, that corresponds to rate of volume increase of about 0.008 m^3/s.
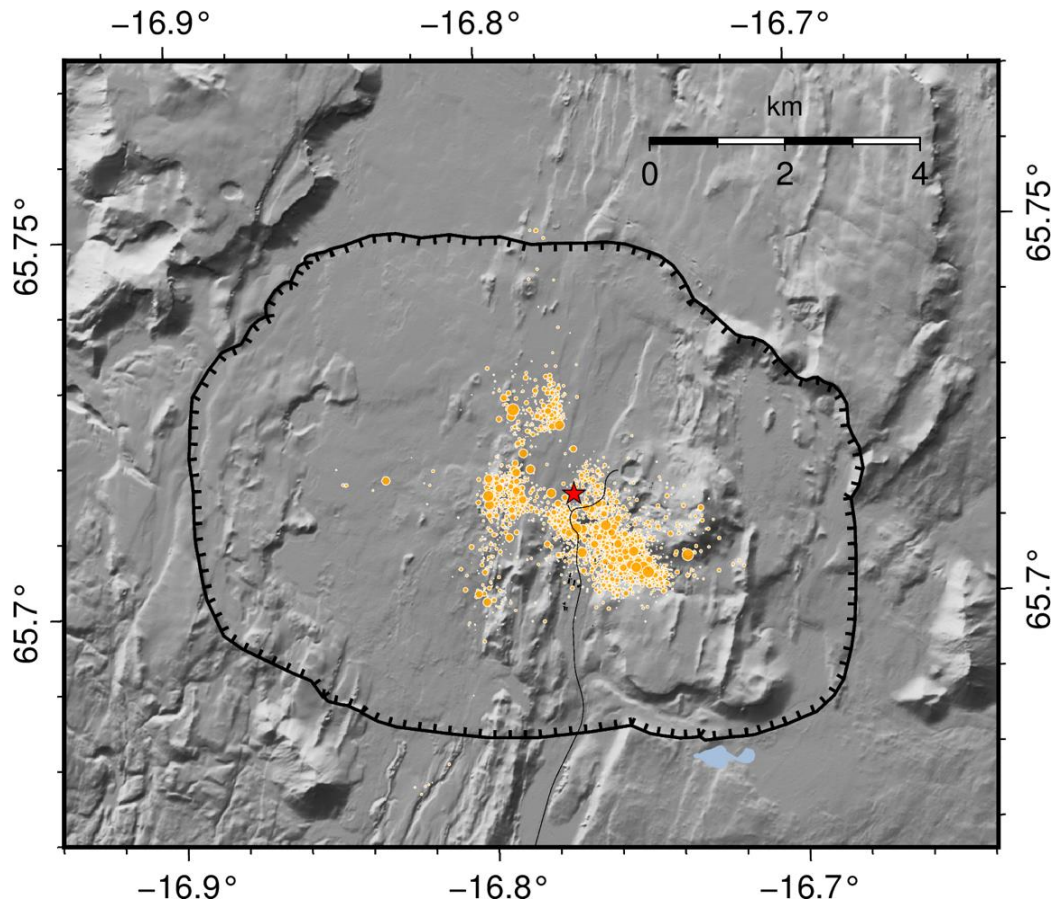
Figure 30. *Location of the best fitting point pressure source model (red star) fitting the 2018-2020 and 2015-2018 difference velocity fields as explained in this report. 95% uncertainty limits about 500 m. The inferred source depth according to the modelling procedure utilized here is 2.2-3.0 km (95% confidence interval). Earthquake activity (double difference relocated events) since the first of July 2018 to August 2020 is also shown (orange circles). Background shows shaded topography, the Krafla caldera boundary (comb line), and roads (black lines).*

The observed change in ground deformation pattern may be related to magmatic or geothermal processes or a combination of both. The depth of the inferred pressure as modelled here is close to the brittle-ductile transition at the inferred location within the caldera and almost directly at or below the bottom of the well IDDP-1 where magma was directly observed just below 2 km depth. This well is, however, abandoned and cemented so it is almost impossible that downflow of fluid in this well can contribute to the pressure source.

Considering uncertainties in the modelling results, and the simplified assumptions made in the modelling process (e.g. the crust is modelled as uniform elastic halfspace, despite material properties may vary significantly), the modelling results should be interpreted with care. The true source of pressure change may originate in the geothermal system, at deeper level within the magmatic system, or at the brittle-ductile boundary where the geothermal and magmatic systems meet.

If the pressure change is of magmatic origin, then inflow of basaltic magma is one possible explanation, at a rate comparable to the inferred average rate of volume increase. A magma inflow rate of 0.008 m^3/s, if comparable to the inferred volume increase at Krafla, is small compared to that inferred in many unrest situations on volcanoes. For example, intrusion at Eyjafjallajökull in 1999, that was part of an 18 years pre-eruptive unrest phase at Eyjafjalla-jökull prior to the 2010 eruption amounted to about 30 million cubicmeters over 6 months, averaging to about 2 m^3/s average volume increase (Pedersen and Sigmundsson, 2006). Another possibility than basaltic magma inflow is taking place, is that pressure increase due to degassing of magma is occurring in the rhyolitic magma body drilled into during IDDP-1.

If the pressure change is of geothermal origin, it can be either because of natural geothermal processes or due to changes in the geothermal utilization. Reversal in ground deformation pattern at volcanoes have sometimes been related to naturally occurring changes e.g. related to earthquakes and changing the flow of groundwater. An example is a suggestion for fracturing of a seal in a geothermal system causing change from inflation to deflation at Yellowstone caldera (e.g., Dzurisin et al., 2012).

Changes in geothermal utilization at Krafla have taken place in recent years that may have contributed to the observed change in ground deformation pattern. Changes have occurred both in the amount of fluid extraction for the Krafla power plant, and the amount and location of fluid re-injection into wells.

Changes in mass extraction from wells relate to optimization of the fluid extraction for the Krafla power plant, by stopping the utilization of wells producing water-rich low enthalpy steam, as dry high enthalpy steam is favored for power production. Each year, observations are conducted at Krafla to measure the productivity of wells. Such measurements show that extraction of mass via utilized boreholes was lower in 2019 than in many preceding years. When measured in summer 2019, mass extracted in wells for the utilization amounted to 226 kg/s, compared to 320 kg/s in summer 2018 (see Table 12 and 13, respectively in Hauksson, 2019). The overall reduction in mass extraction is also evident in Figure 31 that shows evolution of mass extraction divided into steam and liquid water in the 1974-2019 period. In 2019, the amount of liquid water was much lower than in the years before. This is due to closure of water-rich boreholes. When measured in 2018, wells KG-5, KG-24, and KJ-27 stand out as low enthalphy wells (water rich) (Hauksson, 2019). In 2019 they were not in use when the borehole conditions were surveyed. Well 21 had then been added to the network of utilized boreholes.
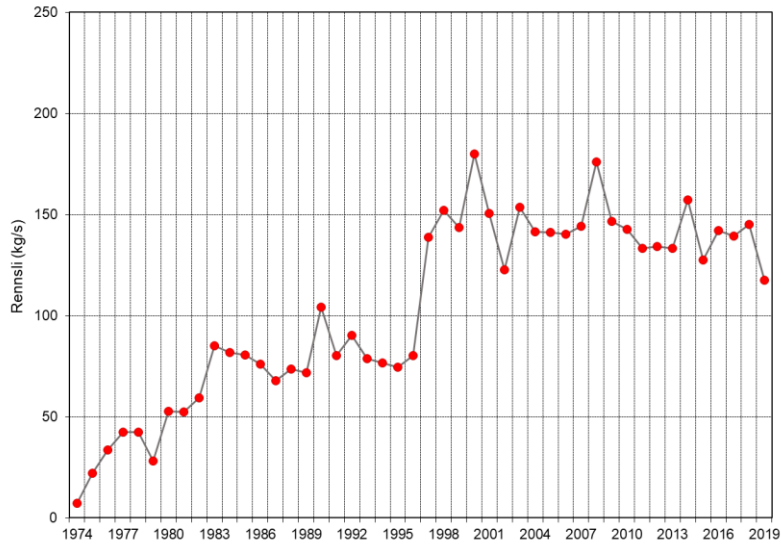
Mynd 34   Samtals gufurennsli úr blásandi borholum í Kröflu.
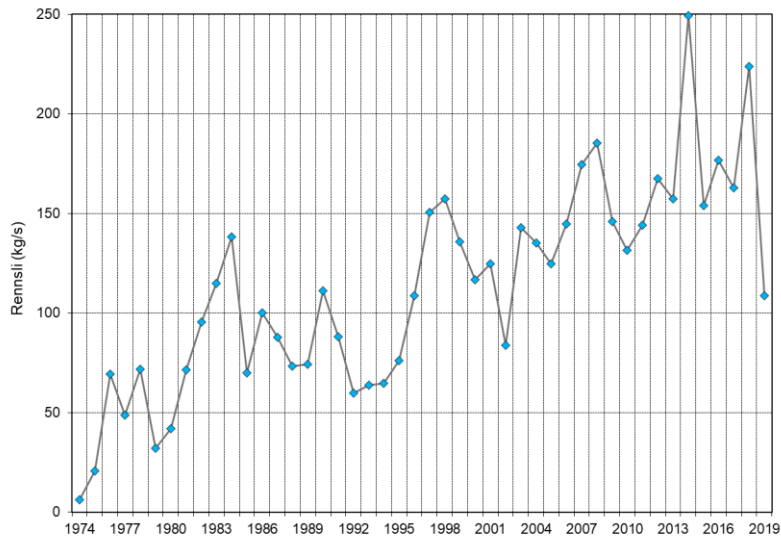
Mynd 35   Samtals vatnsrennsli úr blásandi borholum í Kröflu.

Figure 31. *Total extraction of water from self-flowing wells for the Krafla power plant in kg/s, divided into steam (upper) and liquid water (lower). Reproduced from Hauksson (2020)***.**

Another possible influence on ground deformation is change in re-injection strategy at Krafla. Figure 32 shows the re-injection at three boreholes utilized for that purpose, as well as seismicity during the same period, from January 1st, 2017 to November 1st, 2020. In fall 2018, re-injection began into KJ-35, continuing episodically until middle of 2019. Rate of injection during large part of that interval amounted to about 60 l/s, whereas reduction in injection into well KJ-39 was smaller. Figure 32 also shows the total amount of injection in Krafla. In mid-2019 the injection decreased from around 140 l/s to around 80 l/s.
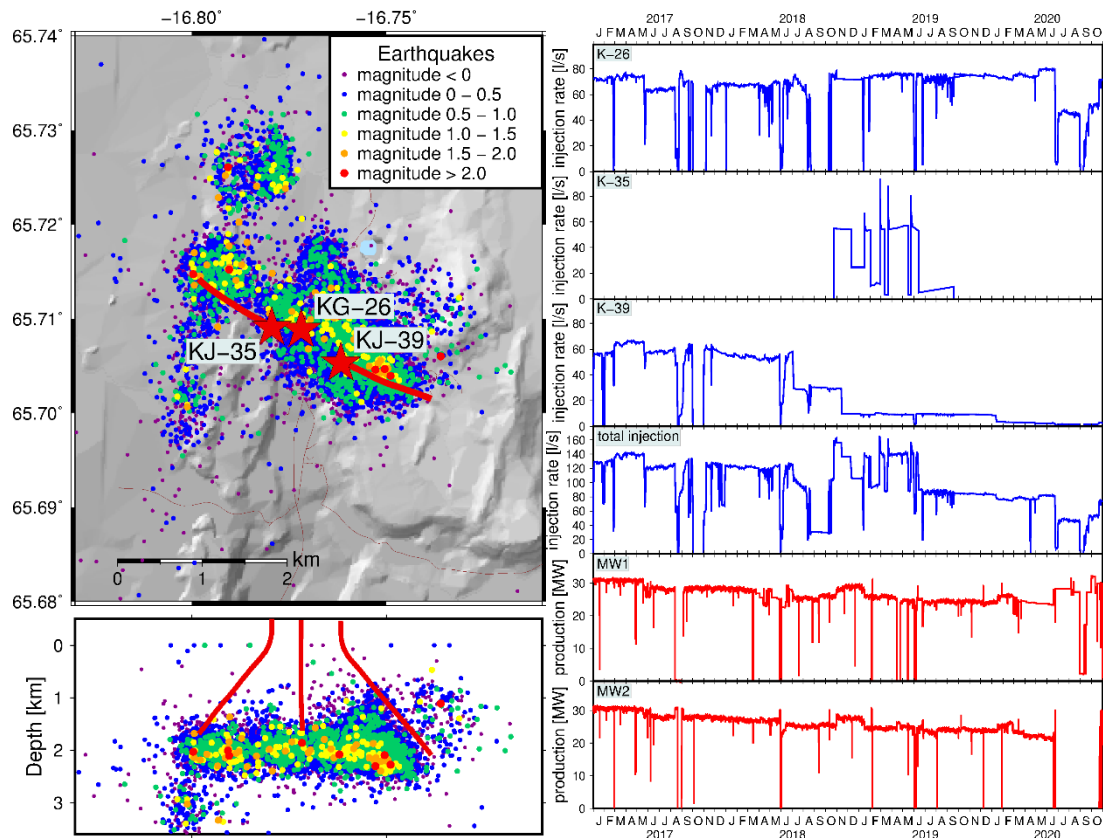
Figure 32. *To the left: The three re-injection wells shown as red stars: KJ-35, KG-26 and KJ-39 overlain on the locations of earthquakes from January 1st, 2017 to November 1st, 2020. Their magnitude is given in the upper right corner. Modified from Blanck et al. (2020). To the right: Re-injection into well KG-26, KJ-35, KJ-39 and the total injection - all from January 2017 to October 2020 in blue and power production in MW at Krafla (engine 1 and 2) in red.*

At the same time as fluid extraction and reinjection have varied, pressure changes have occurred in the Krafla geothermal reservoir. Measurements of pressure and temperature in monitoring well KG-10 at 800 m depth have been carried out yearly (Egilson, 2020). Since 2001, pressure remained stable until 2017 (Figure 33, upper part). When measured in 2018 pressure had increased and continued to increase between the measurements in 2018 and 2019. The increase in the two years interval 2017-2019 amounts to about 0.2 MPa. This change coincides with increase of water level of about 25 m in well KG-10. This does, however, by no means reflect a general 25 m increase of the groundwater level for the Krafla area.

Figure 33 (lower part) shows also the mass extraction history at the Leirbotnar field. The overall net extraction of fluid (extraction minus re-injection) was minimum (lowest value for 40 years). This was due to stop in power production with the second turbine of the Krafla power plant for maintenance purposes (see Figure 32 for power production). This reduction in power production, and associated reduction in fluid extraction in 2020 can be a contributing factor to deformation this year.
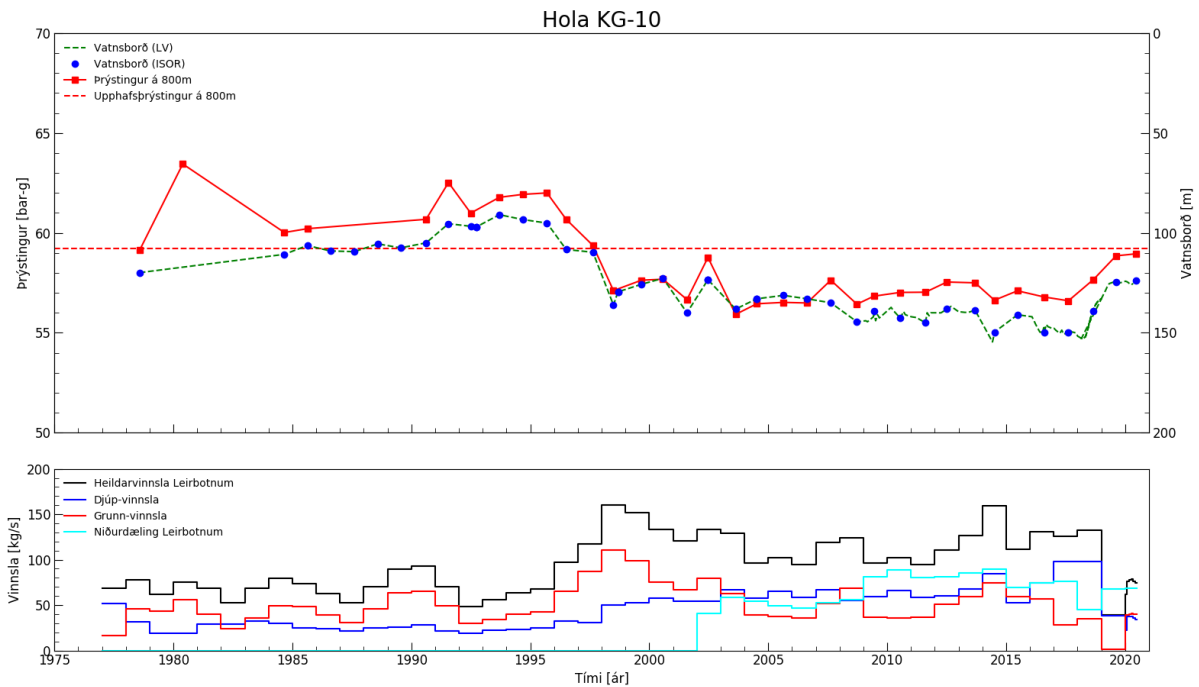
Figure 33. *Borehole data from well KG-10 between 1975 and 2020. Upper part: Pressure at 800 m depth in red and water level in blue. Lower part: History of extraction from the Leirbotnar field, in total (black), from great depth (blue), from shallow depth (red) and re-injection in cyan. Reproduced from Egilson (2020).*

No noticeable changes have been observed so far in the chemical composition of fumarole discharge in the Krafla field that could be related to new intrusives; neither increased concentration of geothermal gases nor volcanic volatiles such as chlorine and boron (Óskarsson et al., 2019). On the contrary, the concentration of carbon dioxide in vapour from Leirhnjúkur has decreased in recent years, even quite sharply since 2017 (Óskarsson and Óladóttir, 2020). Measurements of diffuse carbon dioxide degassing through soil at Leirhnjúkur in the autumn of 2020 do not indicate changes in gas flux through the surface (Óskarsson and Óladóttir, 2020).

7 Conclusion (GPH, FS and KÁ)

After continuous subsidence in the Krafla caldera for many years, inferred inflation of the caldera began in the middle of 2018. InSAR geodetic data 2018-2019 show uplift of 10-13 mm centered on the area between Leirhnjúkur and IDDP-1 well. Between 2019 and 2020, some 8-11 mm additional uplift was observed, centered slightly more to the south, closer to the power station. An additional local deformation signal of 5-6 mm/yr subsidence south of Hvíthólar was inferred in the 2018-2019 period. Continuous GNSS observations at station KRAC south of the Krafla power station show a deformation signal since mid-2018, indicating additional southward movement that presently reaches about 18 mm. Southward displacement at this site corresponds to pressure increase in the crust to the north of the station, as horizontal displacement is expected directly away from the source. Campaign GNSS observations show

also inflation of the Krafla consistent with the InSAR observations, with horizonal displacements broadly aligned outward from the caldera.

The two northernmost gravity sites show negative gravity changes between 2018 and 2019 while most of the others show a positive gravity change. The changes between 2018 and 2019 vary in most cases from 10 μGal to well above 30 μGal. Increase in groundwater level could make these changes. These positive changes are to the south of the uplift and cannot be explained by the processes that cause it.

The difference in ground velocity fields 2018-2020 and 2015-2018 is fitted to a point source of pressure deformation model (Mogi model). Inferred source center depth is ~2.5 km (2.2 – 3.0 km, 95% confidence interval) and the inferred volume change is ~$4.3 \cdot 10^5$ m^3 (3.9 – $6.4 \cdot 10^5$ m^3, 95% confidence interval). These results are dependent on the simplifying assumptions of the model, including no lateral heterogeneities in properties of material hosting the pressure source.

There are significant changes of the seismic activity and the character of seismic release in Krafla during the period from 2018 until autumn of 2020. Fewer and larger events are recorded but energy release increases. First part points to strengthening of the crust and the second part indicates increased energy input in the crust released in earthquakes. The changes occur in steps, some very clear, and the changes seem to be simultaneous with other observed changes, particularly with changes of continuous GNSS observations.

The changes in ground deformation pattern are either related to magmatic or geothermal processes or a combination of both. The depth of the inferred pressure increase is close to the brittle-ductile transition or even within a known magma body. The source of pressure change may originate in the geothermal system, at deeper level within the magmatic system, or at the brittle-ductile boundary where the geothermal and magmatic systems meet.

If the pressure change is of magmatic origin, it may relate to inflow of basaltic magma at a similar rate as the inferred average rate of volume increase. However, the calculated magma inflow rate is small compared to those inferred in many unrest situations on volcanoes. If the pressure change is of geothermal origin, it can be either because of natural geothermal processes or due to changes in the geothermal utilization. In recent years both the amount of fluid extraction and the amount and location of fluid re-injection into wells have changed.

The extraction of mass through utilized boreholes in Krafla was lower in 2019 than during many preceding years. In particular, the amount of liquid water extracted was much lower in 2019 than in the years before due to closure of water-rich boreholes. Re-injection began into well KJ-35 in autumn 2018, continuing episodically until middle of 2019. The total amount of injection in Krafla decreased substantially in mid-2019, from around 140 l/s to around 80 l/s. A pressure increase has been noted in the two year interval 2017-2019 in well KG-10 which amounts to about 0.2 MPa. Finally, no noticeable changes have been observed in the chemical composition of fumarole discharge in the Krafla field that could be related to new intrusives.

8 References

Altamimi, Z., Métivier, L., and Collilieux, X. (2012*). ITRF2008 plate motion model. *Journal of Geophysical Research: Solid Earth, 117(B7).*

Bagnardi, M. and Hooper, A. (2018). Inversion of surface deformation data for rapid estimates of source parameters and uncertainties: A Bayesian approach. *Geochemistry, Geophysics, Geosystems, 19.*

Blanck, H., Ágústsdóttir, Þ., Ágústsson, K. and Gunnarsson, K. (2020). *Seismic Monitoring in Krafla, Námafjall and Þeistareykir.* Iceland GeoSurvey, ÍSOR-2020/003, LV-2020-003.

Drouin, V., Sigmundsson, F., Verhagen, S., Ófeigsson, B.G., Spaans, K. and Hreinsdóttir S. (2017). Deformation at Krafla and Bjarnarflag geothermal areas, Northern Volcanic Zone of Iceland, 1993–2015. *Journal of Volcanology and Geothermal Research, Volume 344*, 92-105. https://doi.org/10.1016/j.jvolgeores.2017.06.013.

Drouin, D., Sigmundsson, F., and Li, S. (2019). *Hægt landris í Kröfluöskjunni 2018–2019.* Memorandum sent to Landsvirkjun on the 18th of October 2019. Iceland GeoSurvey and the University of Iceland. (In Icelandic).

Dzurisin, D. Wicks, C., Poland, M.P. (2012). *History of Surface Displacements at the Yellowstone Caldera, Wyoming, from Leveling Surveys and InSAR Observations*. 1923–2008. USGS Professional paper 1788.

Egilson, Þ., (2020). *Eftirlitsmælingar í Kroflu, Bjarnarflagi og á Þeistareykjum árið 2020*. Iceland GeoSurvey, report, ÍSOR-2020/038 / LV-2020-037. (In Icelandic).

Hanks, T. C. and Kanamori, H. (1979). A Moment magnitude scale. *Journal of Geophysical Research, 84 (B5)*, 2348–50.

Hauksson, T. (2019). *Þeistareykir, Krafla og Bjarnarflag, Afköst borhola og efnainnihald vatns og gufu í borholum og vinnslurás árið 2018*. Report LV-2019-026. Kemía/Landsvirkjun. (In Icelandic).

Hauksson, T. (2020). *Þeistareykir, Krafla og Bjarnarflag, Afköst borhola og efnainnihald vatns og gufu í borholum og vinnslurás árið 2019*. Report LV-2020-010. Kemía/Landsvirkjun. (In Icelandic.)

Herring, T. and McClusky, S. (2009). *GAMIT/GLOBK MATLAB TOOLS.* From: http://www-gpsg.mit.edu/~tah/GGMatlab/#_tsview

Herring, T., R. King, and S. McClusky (2010). *Introduction to gamit/globk, Mas- sachusetts.* Institute of Technology, Cambridge, Massachusetts. https://geo.gob.bo/portal/IMG/pdf/intro_gg_1_.pdf

Hersir, G.P., Vilhjálmsson, A.M., Magnússon, I.Þ., Ágústsson, K. and Drouin, V. (2019a). *Jarðskorpuhreyfingar á Kröflusvæði. Þyngdar- og GNSS-mælingar í nóvember 2019.* Iceland GeoSurvey, Reykjavík, short report, ÍSOR-19067 (In Icelandic).

Hersir, G.P., Ágústsson, K. and Benediktsdóttir, Á. (2019b). *Jarðskorpuhreyfingar á Kröflusvæði – vöktun og mat á ástæðum.* Memorandum sent to Landsvirkjun on the 7th of November 2019. Iceland GeoSurvey. (In Icelandic.)

Lyard, F., Lefevre, F., Letellier, T. and Francis, O. (2006). Modelling the global oceantides: modern insights from FES2004. *Ocean Dynamics, 56*, 394–415

Magnússon, I.Þ. (2016). *Þyngdarmælingar á Þeistareykjum í júlí til september 2015 og þyngdarkort af Kröflusvæði.* Iceland GeoSurvey, Reykjavík, report, ÍSOR-2016/013. (In Icelandic).

Óskarsson, F. and Óladóttir, A.A. (2020). *Leirhnjúkur: Gasstyrkur í gufu og gasflæði um jarðveg.* Iceland GeoSurvey, short report, ÍSOR-20041. ÍSOR/Landsvirkjun. (In Icelandic.)

Óskarsson, F., Ólafsson, M. and Kristinsson, S.G. (2019). *Háhitasvæðin á Þeistareykjum, í Kröflu og Námafjalli. Vöktun á yfirborðsvirkni og grunnvatni árið 2019.* Iceland GeoSurvey, ÍSOR-2019/077, LV-2019-081, 104 pp. ÍSOR/Landsvirkjun. (In Icelandic.)

Portier, N., Hinderer, J. and Bernard, J-D. (2018). *Report on the 2017-2018 relative (Scintrex CG5) micro-gravity measurements at the Theistareykir geothermal plant.* IPGS (Institut de Physique du Globe de Strasbourg), Université de Strasbourg/CNRS, France.

Pedersen, R. and Sigmundsson, F. (2006). Temporal development of the 1999 intrusive episode in the Eyjafjallajökull volcano, Iceland, derived from InSAR images. *Bull. Volc., 68*, 377-393).